Impacts of Temporal and Spatial Variation of Submarine Groundwater Discharge on Nutrient Fluxes to Texas Coastal Embayments

Final Report

TGLO contract number: 17-182-000-9819

NOAA award number: NA16NOS4190174September 2019

Prepared by:
Dorina Murgulet, Principal Investigator

and
Audrey Douglas, Graduate Research Assistant
Cody Lopez, Research Technician
Bimal Gyawali, Graduate Research Assistant
Murgulet Valeriu, Co-Principal Investigator

With assistance from:

William Wolfe, Graduate Research Assistant
Zoe Ruben, Undergraduate Research Assistant
Megan Greige, Undergraduate Research Assistant

Texas A&M University-Corpus Christi
6300 Ocean Dr., Unit 5850
Corpus Christi, Texas 78412
Phone: 361-825-2309
Email: Dorina.murgulet@tamucc.edu

Submitted to:
Texas General Land Office
1700 Congress Ave.
Austin, TX 78701-1495

A report submitted to the Texas Land Commissioner pursuant to National Oceanic and Atmospheric Administration Award No. NA14NOS4190139

Contents

FIGURE LEGEND

TABLE LEGEND

EXECUTIVE SUMMARY

A key goal of this study was to understand the seasonal role of groundwater inflows and nutrient transport to bay systems in south Texas. The ultimate goal was to generate information related to groundwater discharge rates that will improve Environmental Flow recommendations and nutrient criteria in south Texas Estuaries. In average, dissolved organic nitrogen (DON) concentrations in surface water increase from Aransas Bay to Baffin Bay, while dissolved inorganic nitrogen (DIN) concentrations show a different pattern with the highest concentrations Oso Bay in the winter 2017 and 2018 seasons. The highest seasonal average of ammonium concentrations was measured in Baffin Bay followed by Oso Bay. Overall, average nutrient concentrations in porewater follow the same trend across the bays as with surface water. Porewater concentrations of most nutrients were higher than in the water column (silicate, TN, nitrate, phosphate, ammonium). This difference was most pronounced for ammonium, with porewater samples having 10 to 100x higher concentrations than the water column.

The largest submarine groundwater discharge (SGD) rates occurred in Nueces Bay and at the University Beach (seasons average: 109 and 107 cm/d, respectively) and the lowest in Baffin Bay, Laguna Madre and Aransas Bay (seasons average: 15, 19 and 28 cm/d, respectively). Although groundwater discharge rates vary by season at most locations, the average of SGD rates across all bays exhibited very little change between winter 2017 (51 cm/d), spring 2017 (45 cm/d), summer (69 cm/d) and winter 2018 (69 cm/d). On the other hand, nutrient concentrations measured in the interstitial porewater are more variable spatially and temporally. These variations influence the solute fluxes more than the advective SGD rates which, overall, show little seasonal variability**.** The estimates suggest that SGD delivers significant amounts of nitrate in Oso and Baffin bays, summer 2017 and winter 2018 (all seasons average: $65.6*10^3$ and

5.3*10^3 μmol/m^2/day, respectively). The most elevated ammonium fluxes were calculated for Baffin Bay followed by Aransas Bay (all seasons average: 227.8*10^3 and 96.3*10^3 μmol/m^2/day, respectively). Fluxes for all other locations are lower by one order of magnitude when compared to Baffin Bay and about three times lower than Aransas Bay. As in surface and porewater, SGD-derived TOC fluxes increase across the north to south climatic gradient with fluxes rates in Baffin Bay almost twice as high as in Aransas Bay (seasons average: 529.1*10^3 and 290.1*10^3 μmol/m^2/d, respectively). In addition, both silica and phosphate fluxes are similar to concentration trends in porewater and surface water. For instance, the largest overall phosphate fluxes were estimated Oso Bay (seasons average: 10.1*10^3 μmol/m^2/d) and the lowest in Laguna Madre (seasons average: 1.3*10^3 μmol/m^2/d). The largest silica fluxes occurred in Baffin Bay (seasons average: 255.3*10^3 μmol/m^2/d) and the lowest at the University Beach (seasons average: 90*10^3 μmol/m^2/d). This work is critically important for understanding nutrient dynamics in Texas estuaries and helps in setting nutrient criteria by Texas Commission on Environmental Quality (TCEQ) and the US Environmental Protection Agency (USEPA) and improve calibration of groundwater availability models (GAMs) by TWDB.

INTRODUCTION

Background Information

Submarine groundwater discharge (SGD) and coastal groundwater discharge (CGD) are important components of the hydrologic and biogeochemical systems that link terrestrial waters to marine environments (Burnett and Dulaiova 2003; Cardenas et al. 2010; Moore 1996). Submarine groundwater discharge enables the flow and transport of fluids and solutes from terrestrial groundwater sources into offshore coastal embayments (i.e. bays, estuaries, oceans, etc.) whereby coastal groundwater discharge occurs from offshore to inland environments (i.e. wetlands, marshes, etc.). Saltwater intrusion and CGD are similar in their definition and mechanisms of fluid transport; however, CGD assumes that saline groundwater from seawater intrusion will eventually discharge into adjacent surface waters depending upon the hydrogeologic conditions.

Bays and estuaries rely on a specific range of salinity and nutrient levels to maintain optimal productivity and ecosystem services (Palmer et al. 2011). Inflows from riverine and groundwater resources to estuaries are the dominant source of freshwater inflows that can affect coastal ecosystem structure indirectly by changing salinity regimes, hydrology, and transport of nutrients and contaminants. Groundwater, which can accumulate exceptionally high concentrations of nutrients and organic matter, has been shown to contribute to water quality degradation in many coastal systems worldwide (Church 1996). Organic matter-contaminated groundwater discharging to the bays may fuel bacterial respiration, leading to hypoxia formation. It has also been demonstrated that nutrient-contaminated groundwater can fuel growth of phytoplankton and algae in coastal systems. Various coastal systems around the world have experienced and recorded water quality degradation due to nutrient loading from groundwater that can fuel

phytoplankton growth as well as bacterial respiration aiding in hypoxic episodes (Church 1996). In south Texas, several studies are now showing that groundwater represents a significant source of freshwater, nutrients and organic matter, thus it likely plays a major role in ecosystem health (Douglas et al. 2017; Lopez et al. 2018; Murgulet et al. 2015). However, the seasonal changes in groundwater contribution are not well constrained for this area.

In south Texas, severe drought conditions caused depletion of freshwater inflows from riverine sources leading to increased salinity contents in surface waters (Schmidt and Garland 2012). Most studies in south Texas show that impaired waterways are the result of high levels of bacteria or other microbes, dissolved oxygen (DO) depletion, and increasing salinity levels (Montagna and Ritter 2006; Palmer et al. 2011). In Corpus Christi Bay, for instance, formations of hypoxia have cyclically surfaced during the late spring through the fall months (Nelson and Montagna 2009). The upper Laguna Madre Estuary receives no major river discharges. However, this region is nutrient replete and has suffered from a long-lasting bloom of the Texas Brown Tide, which is unusual, and the cause is not fully understood; yet, sources of nutrient are unknown (An and Gardner 2000). In Baffin Bays, as in Corpus Christi Bay, hypoxia symptoms tend to occur during warm summer-fall months. These outbreaks are often related to freshwater pulses which are rich in nutrients and organic matter (unpubl. Texas Parks & Wildlife Spills & Kills Team reports). Given the limited surface runoff contribution to these estuaries during summer and fall, groundwater discharge could be a key factor in delivering nutrients. In fact, the highest nutrients levels in Corpus Christi Bay and Upper Laguna Madre were recorded during lowest precipitation rates in 2014 (Murgulet et al. 2015).

Although monitoring efforts have been extensive, limited efforts were directed towards identifying the quality and quantity of subsurface freshwater and solute inputs to Texas coastal

embayments. Recent efforts to regulate freshwater inflows for optimal salinity ranges to promote ecosystem health of bays and estuaries along the Texas Gulf Coast do not include groundwater inputs (Alexander and Dunton 2006; Kim and Montagna 2012). This project builds upon current efforts to estimate freshwater and nutrient contributions from groundwater to south Texas estuaries which show that groundwater and nutrient discharge changes seasonally likely as a result of hydraulic "heterogeneities", biogeochemical processes, precipitation and inflow sources (i.e. surface vs. subsurface). For instance, SGD-derived nutrient fluxes in Corpus Christi Bay fluctuated spatially between summer and late fall in 2014. While the average SGD rates in the bay were similar among the two seasons, nutrient fluxes increased almost by an order of magnitude by late fall due to a large increase in porewater nutrient concentrations (Murgulet et al. 2015).

Groundwater nutrient concentrations near Oso Bay show elevated levels of nutrients (i.e. 594.3 μmol/L dissolved organic carbon (DOC); 1,814.8 μmol/L total dissolved nitrogen (TDN); 1,606 μmol/L nitrate (NO_3); and 196.8 μmol/L silicate) when compared to surface water. In Copano Bay, during dry conditions, SGD from the 1-km^2 area could supply anywhere between twofold to one order of magnitude more nitrogen (in the form of DIN) than the riverine inputs to Copano Bay. Also, during a wet year SGD equates the river input in the form of DIN alone (Spalt et al. 2018). In Baffin Bay, SGD contributed nutrients up to 3 to 5 orders of magnitude greater than surface runoff; thus, the primary mechanism of nutrient delivery to the bay is SGD (Lopez et al. 2018). These initial studies are indicative of a strong groundwater component that, although patchy, is likely contributing to the water column nutrient concentrations and microbial respiration, at least under the environmental conditions in which the sampling regime took place. However, due to the diffuse and heterogeneous nature of SGD input and the spatial and temporal

variability in groundwater end-member concentrations (caused by variable hydraulic conditions), seasonal monitoring of discharge rates along larger areal extents is necessary to better characterize the system and to project input loads to these systems.

The overall objective of the study is to quantify the spatial-temporal distribution of groundwater and surface water contaminant (nutrients, organic matter) transport and discharge and to evaluate the role of these inputs in system-wide nutrient budgets (i.e., inputs-outputs) across the hydroclimatic gradient of south Texas. To fulfill these objectives, we quantified groundwater discharge and the associated nutrient fluxes on a seasonal basis to the Aransas, Nueces, Corpus Christi, Oso, and Baffin Bays. The resulting data products will aid into the development of decision support products and educational materials that will better equip resource managers and other end users to analyze, detect, and identify potential threats to, and the health of, environmentally sensitive ecosystems such as those of south Texas estuaries.

Study area

The study area encompasses the Aransas, Nueces, Corpus Christi, Oso, and Baffin Bays and the Upper Laguna Madre, located in the coastal bend of Texas (**Figure 1**). These systems are part of watersheds experiencing different rainfall and runoff inputs, and thus, variable freshwater inflows. Laguna Madre, a naturally hypersaline coastal ecosystem located in the area, is one of only three large hypersaline lagoons in the world. This is due to negligible freshwater inflows and little connection with the Gulf leading to high accumulation rates of salt during high evaporation events (Quammen and Onuf 1993). In addition to the climatic gradient, different sources and magnitude of nutrient inputs are expected. For instance, the predominantly low developed land use surrounding these bays result in more pristine conditions in the Aransas Estuary compared to the Nueces and Laguna Madre systems. However, there are emerging

concerns that the ecological health of these vital habitats could be threatened by water quality degradation, specifically pertaining to harmful algae bloom (HAB) (Harred and Campbell 2014). Furthermore, agricultural and other rural practices may contribute nutrients to rivers and groundwater draining into the estuary. The estuary, formed from the drowned Mission and Aransas Rivers, has a direct connection to the Gulf of Mexico at Aransas Pass, but is largely protected by a barrier island, San Jose Island. The estuary receives in average approximately 490,000 acre-feet of freshwater inflow from its major rivers: the Aransas and Mission Rivers, and surrounding drainage basins (TWDB 2017).

The Texas Coastal Plain has a monoclinal belt structure, gently dipping (1.8-7.5 meters (m) per km) toward the Gulf of Mexico (Baker 1979). Bed thicknesses increase down-dip, with sands accumulating approximately 215-400m in the Coastal Bend region (Ashworth and Hopkins 1995). These sediments are ambiguously grouped into the Gulf Coast Aquifer system, a major hydrostratigraphic unit composed of minor sub-units which are difficult to accurately delineate using modern methods (Mace et al. 2006). Sub-units within the system are enriched in uranium deposits, and Texas counties down the hydraulic gradient have increased mortality from malignant neoplasms of respiratory organs, which researchers attribute to increased levels of radon (Rn) and radium (Ra) (Cech et al. 1988). A sole bright side from this occurrence is that it corroborates the use of the uranium-thorium decay series as a groundwater tracer in this area. The estuaries' seafloor is composed of terrigenous and biogenic valley-fill sediments (Mooney and McClelland 2012). Spatial variability of these sediments is related to water depth, proximity to shore, and the underlying geology (Morton and McGowen 1980).

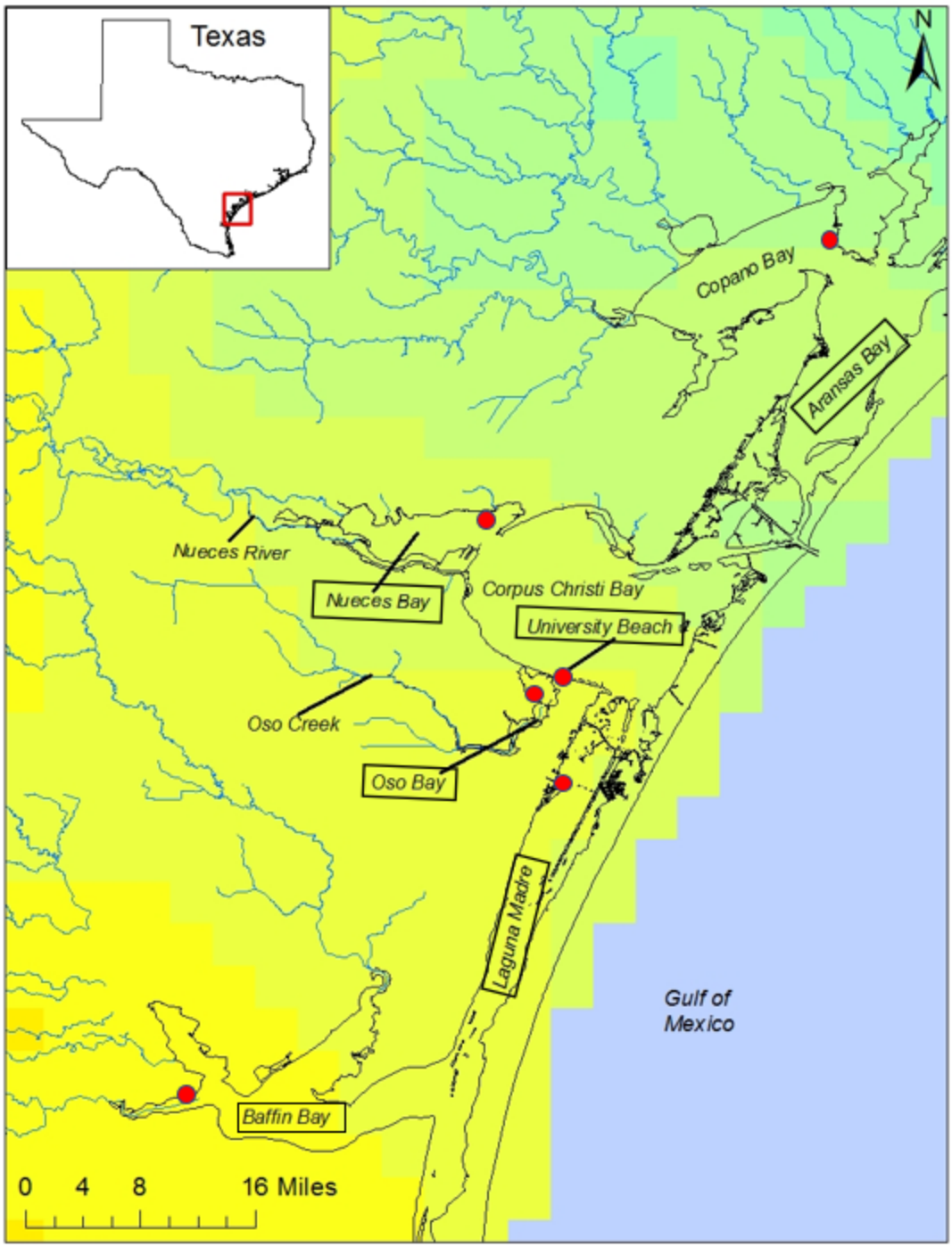

Figure 1. Study areas situated along the south Texas climatic gradient. Sampling sites are denoted by red filled circles.

The bay systems are generally well mixed, in the shallow portions due to elevated local winds, resulting in little stratification under normal conditions. Freshwater inflow to the area is

sporadic and has been connected to highly variable salinities (i.e. fresh to hypersaline) and residence times (i.e. hours for lower river reaches during storms to multiple years for the bay system) (Lebreton et al. 2016). Furthermore, given the microtidal (small tidal range) characteristic, these bays are sensitive to meteorological forcing such as temperature, precipitation and wind. Annual evaporation rates in general exceed the precipitation rates, especially in the further south area including Laguna Madre and Baffin Bay. Tropical storms and hurricanes from the Gulf of Mexico may deliver larger quantities of rainfall during late summer and early fall on an irregular basis (Armstrong et al. 1987), but mostly in the northern reaches of the area (i.e., Nueces and Mission-Aransas estuaries). The dry sub-humid climate on the shallow waters of secondary bays (i.e., Copano, Oso and Nueces Bays) and Baffin Bay manifests not only through reduced freshwater inflows but also increased salinity levels within the bay and estuary system caused by high evaporation rates and salt evapo-concentration (Bighash and Murgulet 2015).

The Gulf Coast Aquifer is a leaky artesian aquifer comprised of a complex of clays, silts, sands, and gravels (Ashworth and Hopkins 1995) that form the Chicot, Evangeline, and Jasper aquifers (Waterstone and Parsons 2003). The estuaries are generally in direct contact with the Chicot aquifer, which is the shallowest of the mentioned aquifers. The stratigraphic units of the Chicot aquifer consist of an overlying alluvial formation preceded by Beaumont and Lissie formations (Ashworth and Hopkins 1995), which are generally composed of clays and clayey silts with intermittent sand and gravel lenses that continue out into the Gulf of Mexico (Waterstone and Parsons 2003). The hydraulic conditions indicate that groundwater flows toward the coast, eventually discharging into the bays and estuaries (Breier et al. 2010; Nyquist et al. 2008; USDA 2012; Waterstone and Parsons 2003).

METHODS

Commonly, analyses of groundwater discharge to surface water has been conducted using elemental and isotopic geochemistry (Burnett 2003; Burnett and Dulaiova 2003; Cable et al. 2004; Dimova et al. 2013; Grossman et al. 2002; Moore 1996; Su et al. 2012) as well as density-dependent flow and transport simulation codes (Guo and Langevin 2002; Murgulet and Tick 2016). Statistical methods such as analysis of variance (ANOVA), multivariate linear regression (MLR) and factor analysis on environmental data have also produced valuable models that aid in identifying variations in water quality and contamination sources in various hydrologic systems (Khan and Kumar 2012; Kim and Montagna 2012; Morehead et al. 2008; Morell et al. 1996; Palmer et al. 2011; Thareja et al. 2011; Voudouris et al. 2000).

Recently, subsurface imaging techniques such as direct current electrical resistivity (ER) surveys have been increasingly used to delineate and quantify groundwater flow paths and discharge rates into surface water bodies (Green et al. 2008; Greenwood et al. 2006; Nyquist et al. 2008; White 1988). Consecutive/continuous ER images acquired along the same survey lines over time periods of hours or during different environmental conditions are used to locate potential groundwater discharge seepage faces and estimate changes in discharge rates over time (Johnson et al. 2012; Nyquist et al. 2008). However, these types of data must be validated by deep core and porewater information. In the absence of field validation data, results are not reliable.

Radon is much more enriched in groundwater when compared to surface waters (typically 1000-fold or greater). Because of its unreactive nature and short half-life ($T_{1/2}$ = 3.83 d) ^{222}Rn is an excellent tracer to identify areas of significant groundwater discharge (Burnett and Dulaiova 2003). Recent studies demonstrate that continuous radon measurements could provide

reasonably high-resolution data to evaluate changes of radon concentration of surface water at one location over time (Burnett and Dulaiova 2003; Burnett et al. 2001).

In this study, we are applying a combination of geochemical methods to trace and quantify groundwater discharge to the south Texas estuaries across seasons and changing hydroclimatic conditions. The hydroclimatic conditions encountered during the sampling period vary from north to south as shown in **Figure 2**. Samples were collected from the six bays during four sampling periods which for discussion purposes will be referred to as: winter 2017 (December 2016-January 2017), spring 2017 (April-June 2017), summer 2017 (August-September 2017), and winter 2018 (December 2016-January 2018). Only one wet period was captured during the study, the summer 2017 event. However, only the Aransas and Nueces Estuaries are receiving higher streamflow and precipitation. The Laguna Madre and Baffin Bay encounter similar conditions throughout the four seasons, except of course for temperature and evaporations rates which change seasonally (not shown in **Figure 2**). Wind speed conditions go consistently above 5 m s^{-1} with gusts as high as 15 m s^{-1}. Sampling and monitoring of radon were dependent on wind conditions, but generally occurred during calm days. For this reason, field surveys for each season extended over periods of two months.

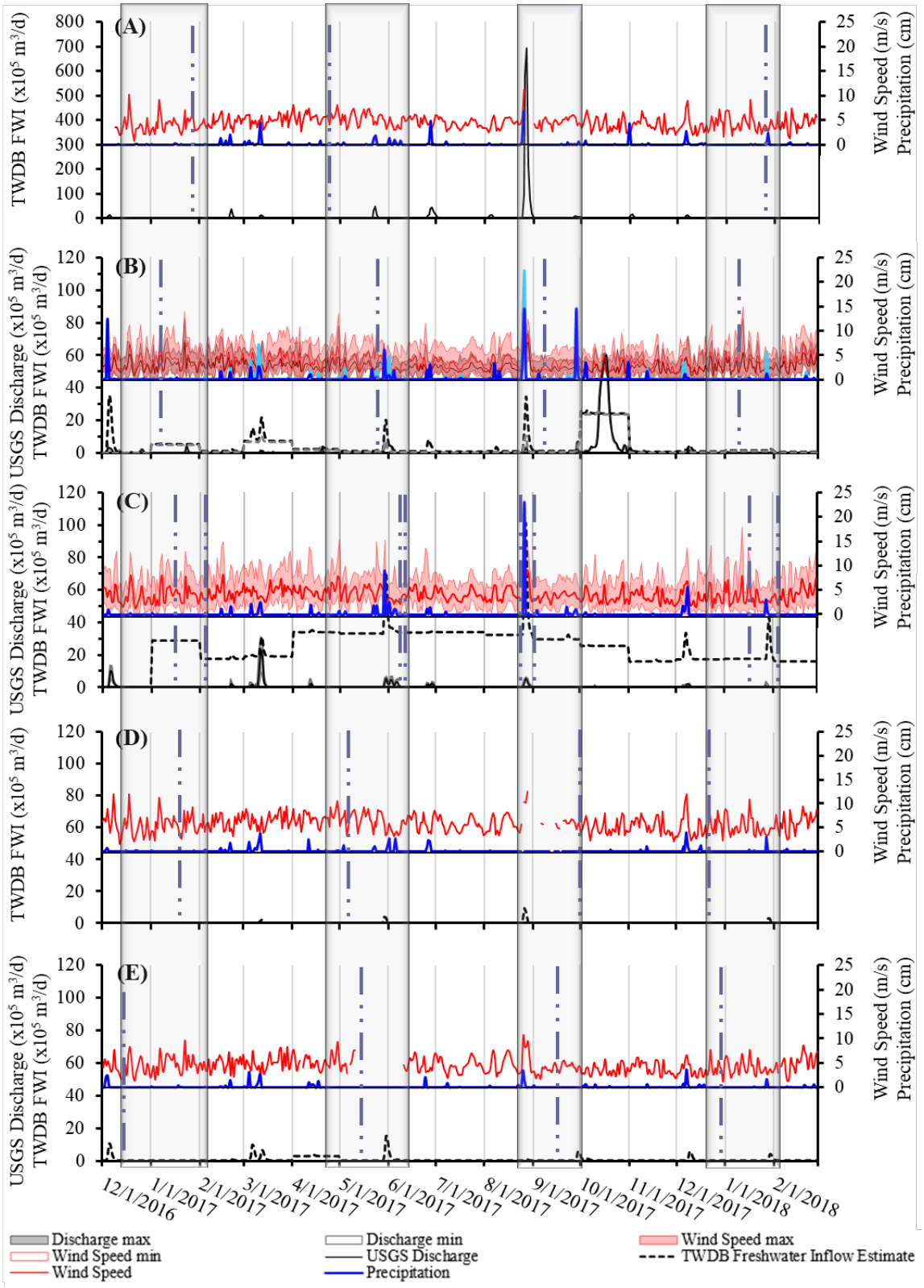

Figure 2. Hydroclimatic conditions encountered during the sampling period for (A) Aransas Bay, (B) Nueces Bay, (C) Oso Bay and University Beach, (D) Laguna Madre, and (E) Baffin Bay. Vertical grey bars outline each sampling event and vertical dash-dot-dot lines indicate when

sampling occurred in each bay. Included are: stream discharge from USGS gauges 08211500 (Nueces River), 08211520 (Oso Creek), and 08212400 (Los Olmos Creek) (USGS 2019); modeled surface runoff from TWDB Freshwater Inflow Estimates (TWDB 2019) for subwatersheds 20130, 20165, 20180, 20192, 20194 (Aransas Bay), 20005, 21010, 22012 (Nueces Bay), 22011, 22014, 22015 (Oso Bay and University Beach), 22026 (Laguna Madre), and 22040 (Baffin Bay); and precipitation and wind speed from NOAA National Climate Data Center (NOAA 2019) stations USW00012972 (Aransas Bay), USW00012926 (Laguna Madre), and USW00012928 (Baffin Bay) and from Corpus Christi Meteorological Stations #7, Del-Mar West (Nueces Bay), and TAMUCC (Oso Bay and University Beach) (CBI 2019).

Water Sample Collection

Continuous electrical resistivity (continuous resistivity profiles) surveys conducted as part of previous projects were used to identify the most relevant submarine groundwater discharge sites in each of the bays. Briefly, one location was selected in each of the bays as follows: Goose Island in Aransas Bay, Nueces Bay along the north shore, University Beach in Corpus Christi Bay, Oso Bay at South Bay Park, upper Laguna Madre, and Baffin Bay. After selection of time series monitoring sites, time-lapse resistivity surveys were conducted at the same time with the water data collection to constrain SGD rates.

Discrete porewater (where field conditions allowed it) and surface water samples were collected at each time-series station dependent on the subsurface and bottom sediments characteristics. For instance, in Nueces Bay we have encountered portions where the bottom sediment was completely saturated and in suspension for several meters below the sediment water interface while at other locations, a hard clay layer was encountered a few centimeters below the interface. The former is evidence of potential location for SGD. Surface water samples were collected from within the water column at about 0.2 m above the water-sediment interface. Dependent on accessibility and field conditions, attempts were made to collect resistivity images along water-land transects to better define the direction of groundwater flow (define flowpaths). However, translation to SGD rates was not possible because of lack of deeper porewater and

stratigraphic information to constrain changes in the electrical resistivity. For that purpose, these images are not included in this report.

Samples from the water column were collected using a Van Dorn water sampler deployed to the desired depth and given a few minutes to allow water to circulate throughout the cartridge. Sampling bottles are rinsed three times and then overfilled, capped, and placed on ice depending on the required procedure for each analyte. A porewater sampler (AMS Retract-a-Tip) was used to collect porewater samples. The porewater sampler consists of 1 m sections of hollow steel pipe attached to a retract-a-tip point that is inserted about 0.2 to 1 m below the sediment-water interface. The depth of sample extraction is critical to sampling to prevent bottom waters from contaminating porewater samples (RCRA 2009). The sample is extracted using a peristaltic pump attached to silicone tubing which is connected to the retract-a-tip at the other end. Before sample collection the silicone tubing is purged until the sample is clear (or a minimum amount of sediment is present in the sample) and field parameters (i.e. salinity, temperature, pH) stabilize.

The following parameters were measured: continuous radon-222 (^{222}Rn); radium-224 (^{224}Ra); radium-226 (^{226}Ra); chlorophyll-α (chl-α); nutrients (ammonium, nitrate + nitrite, nitrite); dissolved inorganic carbon (DIC); dissolved organic carbon (DOC); hydrogen, oxygen, and carbon stable isotopes (δD, δ^{18}O, and δ^{13}C, respectively) nitrogen and oxygen isotopes of nitrate (δ^{18}O and δ^{15}N, respectively). Dissolved oxygen (DO), salinity, temperature, pH, specific conductivity readings were obtained at each sampling site before sample collection using an YSI multiparameter water quality meter. The YSI meter was placed at each sampling depth within the water column for several minutes to allow proper circulation of sample and instrument stability before parameters were recorded. Observations of any potential sources of contamination and additional watershed characteristics such as land use will be noted. Water samples were collected

in compliance with standard sampling techniques (Brown et al. 1970; RCRA 2009; Wood 1976). At each location, the water depth was measured using a pre-labeled line attached to a weight.

Stable Isotope Sampling

Samples for measurements of stable isotope ratios of oxygen ($\delta^{18}O$), hydrogen (δD), and carbon stable isotope ratio of DIC ($\delta^{13}C$) were collected using the above procedure. Abundances of oxygen, hydrogen and carbon isotopes were measured (with an uncertainty of ±1per mil (‰) for δD, ± 0.1 for $\delta^{18}O$, and ± 0.2 for $\delta^{13}C$) relative to accepted international standards, which are the Vienna Standard Mean Oceanic Water (VSMOW) (for oxygen and hydrogen) and the Vienna Pee Dee Belemnite (VPDB) (for carbon).

Alkalinity and DIC samples were collected in 250 mL borosilicate bottles with no head space and preserved using 100 microliters (µL) of saturated mercuric chloride ($HgCl_2$) (Kattner 1999). Total alkalinity (TA) was processed by Gran titration utilizing an automatic titrator with an attached temperature control water bath maintained at 22 ^oC and a pH electrode. Hydrochloric acid (HCl) was used as the titrant with a concentration of approximately 0.1 moles per liter (mol/L). Alkalinity samples were run multiple times to reach a precision of 0.1% (Cyronak et al. 2013).

Nutrient and Chlorophyll-α Sampling

For simplicity, we computed the average and minimum and maximum for each parameter of interest for all regions as explained in the 'Spatial-temporal Distribution of Phytoplankton and Nutrients' section. Water samples were collected in acid-washed amber polycarbonate bottles using the techniques mentioned above. Bottles were stored on ice until return to a shore-based facility where processing of samples occurred, and analyses were conducted for chlorophyll-α

(surface water) and nutrients and organic matter (surface water and porewater). Chlorophyll-α was determined from samples collected on and extracted from Whatman GF/F filters (nominal pore size 0.7 μm). Chlorophyll was extracted using 90% acetone and analyzed fluorometrically. Inorganic nutrients (nitrate + nitrite (N+N), nitrite, silicate, orthophosphate, ammonium) were determined in the filtrate of water that passed through 0.2 μm filters using a Seal QuAAtro autoanalyzer. Measurements of total organic carbon (TOC) and total dissolved nitrogen (TN) were determined in the filtrate of water that passed through the 0.2 filters using a Shimadzu TOC-V analyzer with nitrogen module. DON for surface water was estimated as the difference between TN and inorganic nitrogen.

Radiogenic Isotopes

Sampling and lab measurements

Samples for radium isotope measurements were collected in three-20L jugs at each of the monitoring stations at the beginning and end around every tidal change. The samples were filtered in the field using a 1μm and a 0.5μm sequence of filters. Next, filtered samples were processed through ~15g fluffed manganese dioxide, MnO_2, impregnated acrylic fibers twice at a rate of <1L/min (Dimova et al. 2007; Kim et al. 2001). Following, the Mn-fibers were rinsed with Ra-free water, to eliminate any salts or particulates, and then pressed to a water to fiber ratio of 0.3-1g (i.e., 20-30g wet weight) (Sun and Torgersen 1998). Next, the fibers were placed in gas-tight cartridges and tested for ^{223}Ra and ^{224}Ra on a Radium Delayed Coincidence Counter (RaDeCC), which were done within three days of collection (Moore 2006).

After measurements of the above-mentioned short-lived isotopes, fibers were flushed with nitrogen gas and sealed for >21days to reach secular equilibrium before measuring ^{226}Ra. The ^{226}Ra samples were run on a RAD-7 with measurements corrected to a calibration curve

determined from 5 standards. Measurements of ^{222}Rn from porewater and groundwater grab samples were conducted using a *Durridge RAD-7* radon-in-air monitor and the RAD AQUA accessory. The RAD AQUA is used to bring the radon concentration in a closed air loop into equilibrium with the radon concentration in a flow-through water supply. This method was also used for continuous measurements of radon in water that are used to calculate groundwater discharge rates as descried in the next section.

Extraction efficiencies of Mn fibers were determined to be 99% for ^{223}Ra, 98% for ^{224}Ra and 96% for ^{226}Ra by processing random samples through a second Mn cartridge. For ^{224}Ra and ^{223}Ra, the presented uncertainty is the maximum expected of 10% efficiency for RaDeCC measurements. However, much lower uncertainties were observed as all counts exceeded 100. Analytical errors, determined from RAD-7 counting statistics, were less than 8% for ^{226}Ra at the 95% confidence interval.

Submarine groundwater discharge flux calculations

Radon-derived SGD rates

Continuous measurements of ^{222}Rn were conducted at the six selected locations throughout the south Texas estuaries. The automated radon system (RAD-7 and the RAD AQUA accessories) was placed at the end of peers, about 100 m offshore or on the deck of the research vessel (i.e., the Laguna Madre). The monitoring system measures ^{222}Rn from a constant stream of water (driven by a peristaltic pump) passing through an air-water exchanger. The exchanger distributes radon from a running flow of water to a closed air loop that fees to the RAD-7 radon-in-air monitor. A detailed description of RAD-7 capabilities and measurement principles can be found in (Burnett and Dulaiova 2003). Radon measurements were integrated over 30-minute intervals.

The main principle behind using continuous radon measurements to quantify groundwater discharge rates to surface waters is based on the inventory of ^{222}Rn over time accounting for losses/gains due to mixing with waters of different radon concentrations (i.e. low concentrations offshore waters), atmospheric evasion, and sediment inputs. Thus, changes over time, if any, can be converted to radon fluxes. Using the advective fluid activities (e.g., porewater or groundwater activities as the endmember), the ^{222}Rn fluxes are converted to water fluxes following methods described by Burnett and Dulaiova (2003).

Monitoring of radon extended over 12 to 24 hours at most stations, depending on weather conditions (e.g., at winds of more than 12 miles per hour bay conditions become very difficult for sampling and data collection). Exception is the Laguna Madre, where the time series data collection occurred over 6-8 hours. Data collection at this station was at a distance from the shore, off a boat, thus the sampling times was constrained by daylight and wind conditions. Thus, tidal effects were addressed at some locations; although, changes in water levels of no more than 0.2 meters are recorded in this area due to tidal fluctuations (NOAA 2014). It is assumed that the lower radon fluxes observed during the monitoring time are due to mixing with offshore waters of lower concentration and wind effects (i.e., radon degassing).

The maximum absolute values of the observed negative fluxes during each time-series event at each location are used to correct radon fluxes for losses via mixing. However, there are concerns that atmospheric evasion due to persistent winds are not accurately reflected in the radon mass-balance (see Spalt et al. (2018) for information of effects of degassing on SGD rates). Sediment-supported radon concentrations were measured using laboratory equilibration experiments from sediment cores collected at each time-series station following the methods outlined by Corbett et al. (1998). Sediment samples (i.e. 2 cm) collected from every 10 cm of

the cores were placed into a 500ml Erlenmeyer flask, equilibrated with 400mL of Ra-free bay water, sealed, and after agitation on a shaker table for >21 days, were analyzed for the amount of ^{222}Rn that escaped into the fluid phase. This provides the sediment equilibrated ^{222}Rn concentration (or sediment-supported ^{222}Rn) for each SGD site. Finally, we calculate water fluxes (q, cm/d) by dividing the total estimated ^{222}Rn fluxes (T_{total}, $Bq \cdot m^{-2} \cdot s^{-1}$) by the concentration of ^{222}Rn ($^{222}Rn_{gw}$, $Bq \cdot m^{-3}$) in the fluids entering the system (Burnett and Dulaiova 2003).

Radium-derived SGD rates

Radium-based SGD estimates, representative of the potion of the bay where measurements were conducted (Charette et al. 2001), were determined using water ages derived from the longer-lived ^{226}Ra and ^{223}Ra ages, stream discharge (i.e., freshwater inflow estimates) (TWDB (Texas Water Development Board) 2016), and the porewater ^{226}Ra and ^{223}Ra measurements as the source endmember.

Relative water mass ages

Activity ratios (AR) of ^{224}Ra:^{226}Ra were estimated for each sampling station to estimate relative radium ages for SGD calculations (Peterson et al. 2008). Relative radium age of the surface water, or the relative time (T_r) that has passed since the radium first entered the system in a well-mixed estuary, and therefore has been separated from its radionuclide source (i.e., subsurface sediments), was calculated using the ratio of the short-lived ^{224}Ra to the long-lived ^{223}Ra and ^{226}Ra isotopes using equation 1 (Knee et al. 2011):

$$T_r = \frac{AR_{GW} - AR_{CO}}{AR_{CO} \times \lambda_{224}} \quad (1)$$

where AR_{GW} is the initial activity ratio of discharging groundwater, AR_{CO} is the measured activity ratio at the station of interest, and λ_{224} is the decay constant (d^{-1}) for the short-lived ^{224}Ra isotope.

This equation assumes radium activities and ARs are greatest in the radium source (i.e., groundwater or porewater containing radium) and in the receiving nearshore water, relative to offshore due to SGD input and desorption from sediments. Consequently, radium activities and ARs should be decreasing as the water mass is moving away from the discharge point. This could occur due to two reasons: radioactive decay and mixing with more dilute offshore waters. This equation also assumes that radium additions are occurring continuously over a wide area, which in this case is the entire bay, with multiple groundwater discharge locations. For instance, the short-lived isotope (i.e., ^{224}Ra) is normalized to the long-lived isotope (i.e., ^{226}Ra) with activities that are expected to only decrease due to dilution.

Desorption laboratory experiments using sediment cores at several locations show that the flux of dissolved ^{226}Ra from bottom sediment alone (0.02 $Bq \cdot m^2$) are negligible for this study (see section 4.3.1). Therefore, we can assume that the major input of ^{226}Ra comes from SGD rather than from sediment diffusion or resuspension, thus, excluded from the mass balance (see eq. 2). Sediment supported ^{223}Ra activities were not measured in this study. Because the half-life of ^{226}Ra is much longer ($t_{½}$ = 1,600 yr) with respect to mixing time, its decay rate may be neglected, however for ^{223}Ra the half-life must be considered based on the time estimated as the radium age. Using the groundwater activity ratios as the source of radium (i.e., water source), an estimate of the time since SGD occurred is provided. The radium age is not to be confused with the bay water residence time, which reflects the amount of time water resides in the bay before it

is flushed out. They can, however, provide knowledge related to how fast water moves through the porous media as they are used to calculate SGD rates (Swarzenski et al. 2007).

Radium mass-balance and submarine groundwater discharge estimates

To estimate SGD from ^{226}Ra or ^{223}Ra observations ($^{226/223}$Ra) in Baffin Bay, an estuarine mass balance was developed to determine the excess ^{226}Ra (due to groundwater flux) in the bay. This includes all sources of radium other than groundwater, including tidal exchange, riverine input, desorption from riverine suspended sediments, and diffusion from bay bottom sediments (Moore 1996). Expressed mathematically, excess ^{226}Ra ($^{226}Ra_{ex}$ [Bq·d^{-1}]), or ^{223}Ra ($^{223}Ra_{ex}$ [Bq·d^{-1}]) thereof, in the bay equals:

$$^{226/223}Ra_{ex} = \left[\frac{\left(^{226/223}Ra_{Bay} - ^{226/223}Ra_{sea}\right) \times V_{bay}}{T_r}\right] \quad (2)$$

where $^{226/223}Ra_{Bay}$ is the average measured ^{226}Ra, or ^{223}Ra, activity in the bay; $^{226/223}Ra_{sea}$ is the average ^{226}Ra, or ^{223}Ra, activity in the offshore water body (i.e., Laguna Madre in the case of Baffin Bay), which exchanges tidally with the bay of interest; V_{bay} is the volume of the bay of interest; T_r is the residence time, or flushing rate, estimated from the apparent radium water ages (i.e., equation 1). It is assumed that the excess activity from equation (2) is the result of SGD. Thus, using a porewater endmember activity ($^{226/223}Ra_{PW}$), SGD is calculated from:

$$SGD_{^{226/223}Ra} = \frac{^{226/223}Ra_{ex}}{^{226/223}Ra_{PW}} \quad (3)$$

RESULTS AND DISCUSSIONS

Alkalinity, DIC and $\delta^{13}C$

Total alkalinity concentrations in surface water vary both temporally and spatially (**Table 1)**. The lowest overall TA and DIC concentrations and most depleted $\delta^{13}C$ were measured in Oso Bay. By season, the lowest TA and DIC concentrations were measured in late spring, followed by summer also in Oso Bay (**Table 1**). This bay also experienced the most depleted $\delta^{13}C$, except of one occurrence in Baffin Bay in late spring, with a $\delta^{13}C$ value of -16.5‰. The highest overall TA and DIC were measured in Baffin Bay followed by Aransas Bay. Nueces Bay and University Beach (in Corpus Christi Bay) also exhibit lower TA and DIC, overall. While higher TA and DIC are expected at the low salinity end, in this study, they occur at the high-salinity end in Baffin Bay. As a matter of fact, the only observed decrease in salinity that can be associated with higher rates of precipitation and river discharge in Oso Bay, in late summer, is not associated with an increase in TA or DIC or decrease in salinity. Some riverine influence on TA and DIC may be observed in Aransas Bay in spring and winter, while not much influence is observed for the other bays. No freshwater influence is observed for Baffin Bay for any of the four seasons (**Table 1; Table 3**).

TA consumption in surface water Oso Bay is not evident during the winter 2017 and 2018 events when concentrations are more elevated than the Nueces Bay and University Beach. Although differences across the bay system are not extremely large, except for Oso Bay, there is a significant amount of heterogeneity across the climatic gradient, especially in the Oso and Baffin Bay which are at the opposite extremes, particularly during the spring and summer events (**Table 1)**.

Porewater TA and DIC (**Table 2**) are in general higher than surface water, with the largest concentrations measured consistently in Baffin Bay and Laguna Madre, followed by Aransas Bay and Oso Bay. In Baffin Bay, the largest TA and DIC concentrations were found in winter 2017. In this bay, all other seasons are very similar in concentrations but, in average, three-fold smaller than winter 2017, (**Table 1).** In addition, winter 2017 porewater TA and DIC concentrations were also higher when compared to the other 3 seasons in Oso Bay while Laguna Madre exhibited similar concentrations winter, spring and summer 2016, but dropped by almost 1,000 μM by winter 2018.

In average, the most depleted $\delta^{13}C$ signatures were measured in Aransas Bay (average min: -11.9‰) followed by Baffin Bay (average min: -6.9‰) and Oso Bay (average min: -6.4‰). The most enriched signatures were measured in Nueces Bay and University Beach (average max: -3.5‰ and -3.6‰, respectively). Seasonally, the most depleted $\delta^{13}C$ signatures were measured in Aransas Bay in spring 2016 (-22.7‰) while the most enriched in Nueces Bay (-2.6‰), in winter 2017. Across all bays, the most enriched signatures were found in winter 2018 (**Table 2**). Thus, in general, more depleted signatures are associated with higher TA and DIC in each bay, but this observation is not true when all bays are considered. For instance, the most negative signature in Aransas Bay is associated with the most enriched TA and DIC for that bay, but not with the largest TA and DIC concentrations overall. Though, the more depleted $\delta^{13}C$ could be more correlated with lower salinities (**Table 2**). Porewater salinities increase from Aransas Bay to Baffin Bay with just a few exceptions at University Beach in summer 2016. Nueces Bay, University Beach and Oso Bay have very similar salinities ranging anywhere between 26.8 to 31.0. There is a two-fold increase in the average of all season's salinity between Aransas Bay (19.3) and Baffin Bay (46.1) (**Table 4**). Even between the two adjacent northern bays, Aransas

and Nueces Bays, salinity increases approximately by a factor of 0.5 (i.e., 19.3 to 28.5, respectively). This behavior is closely emulated by surface water salinities, not only as far as trends go, but level of salinity as well (**Table 3**; **Table 4**).

Table 1. Surface water values of alkalinity (Alk., μM), dissolved inorganic carbon (DIC, μM), $\delta^{13}C$ (‰), $\delta^{18}O$ (‰), deuterium (δD, ‰) for all the bays of interest during each sampling event presented as the minimum, maximum, and average value. Overall average for each parameter is also provided. † Winter 2017 NB samples were collected from station 7 from Murgulet et al. (2018). ‡ Winter 2017 BB samples are from station 11 from Lopez et al. (2018).

		AB			NB†			UB			OB			LM			BB‡		
		Min.	Max.	Avg.	Min.	Max.	Avg.	Min.	Max.	Avg.	Min.	Max.	Avg.	Min.	Max.	Avg.	Min.	Max.	Avg.
December 2016 - January 2017	Alk.	3060	3307	3169	2618	2721	2657	2682	2806	2737	2931	3057	3001	3180	3193	3189	3893	3949	3927
	DIC	2611	3022	2892	2328	2379	2356	2386	2548	2437	2514	2782	2673	2844	2906	2878	3252	3286	3276
	$\delta^{13}C$	-5.27	-2.15	-4.22	-1.99	-1.68	-1.87	-1.72	-1.01	-1.42	-2.36	-0.73	-1.34	-1.41	-0.95	-1.25	-2.79	-1.55	-1.96
	$\delta^{18}O$	-0.14	1.74	0.38	1.31	1.48	1.42	0.52	1.30	1.12	0.77	2.39	1.59	1.02	1.77	1.27	1.23	2.45	2.16
	δD	-0.26	9.22	7.06	10.35	11.09	10.78	5.61	10.85	9.60	4.25	17.01	13.58	9.91	11.96	10.45	12.71	21.04	18.78
April - June 2017	Alk.	2834	3091	2970	2585	2649	2626	2566	2633	2588	1925	2042	1991	3046	3071	3058	3377	3555	3493
	DIC	2395	2786	2622	2190	2335	2258	2176	2356	2235	1441	1738	1592	1995	2164	2107	2713	3002	2902
	$\delta^{13}C$	-3.62	-1.77	-2.95	-4.47	-0.75	-1.69	-2.24	-1.17	-1.78	-4.65	-1.85	-3.20	-2.33	-1.71	-1.97	-16.49	0.15	-1.54
	$\delta^{18}O$	0.44	2.01	1.37	-0.23	2.58	1.64	0.50	2.17	1.13	-1.69	0.12	-0.65	1.93	4.32	2.74	1.49	3.95	2.43
	δD	2.19	14.53	9.32	7.64	14.84	11.70	2.79	15.40	8.22	-9.45	-4.67	-6.61	10.74	29.88	16.37	4.25	30.79	16.44
August - September 2017	Alk.	Goose Island State Park closed due to Hurricane Harvey damage.			2540	2635	2586	2679	2809	2739	2299	2428	2365	2659	2808	2738	3377	3530	3449
	DIC				2093	2221	2163	1974	2532	2234	1834	2097	1947	2251	2438	2349	2664	2882	2760
	$\delta^{13}C$				-2.84	-0.88	-1.54	-3.06	-0.77	-1.75	-4.41	-2.64	-3.47	-2.26	-0.55	-1.33	-4.43	0.13	-1.00
	$\delta^{18}O$				-0.15	2.62	0.76	-1.00	3.21	1.40	-4.21	-2.63	-3.54	-0.26	0.85	0.22	0.78	3.15	2.34
	δD				-4.26	3.87	-0.09	0.80	18.61	11.73	-32.23	-21.94	-27.71	-0.76	7.33	4.06	5.91	21.64	13.86
December 2017 - January2018	Alk.	2684	2959	2848	2561	2798	2634	2609	2670	2642	2566	3532	2925	2685	2736	2712	3507	3566	3531
	DIC	2533	2748	2641	2387	2570	2475	2356	2428	2398	1313	2528	2147	2370	2447	2410	2917	2990	2958
	$\delta^{13}C$	-3.15	-2.50	-2.76	-2.42	-1.76	-2.17	-1.93	-1.36	-1.64	-4.12	-2.38	-3.36	-1.35	-0.90	-1.14	-2.46	-1.99	-2.19
	$\delta^{18}O$	-2.35	-0.18	-1.20	-1.14	2.93	0.37	-3.12	1.46	-0.47	-2.03	1.19	-0.64	-1.03	0.85	-0.30	-1.97	2.19	0.79
	δD	-7.12	2.00	-2.01	-2.29	11.20	5.45	-6.27	5.23	1.24	-10.43	9.13	-0.04	-3.38	6.07	2.10	-7.19	14.12	8.48
Overall Avg.	Alk.	2859	3119	2996	2576	2701	2626	2634	2730	2677	2430	2765	2570	2893	2952	2924	3539	3650	3600
	DIC	2513	2852	2718	2249	2376	2313	2223	2466	2326	1775	2286	2090	2365	2489	2436	2886	3040	2974
	$\delta^{13}C$	-4.01	-2.14	-3.31	-2.93	-1.27	-1.81	-2.24	-1.08	-1.65	-3.89	-1.90	-2.84	-1.84	-1.03	-1.43	-6.54	-0.81	-1.67
	$\delta^{18}O$	-0.68	1.19	0.18	-0.05	2.40	1.05	-0.77	2.04	0.80	-1.79	0.27	-0.81	0.41	1.95	0.98	0.38	2.94	1.93
	δD	-1.73	8.58	4.79	2.86	10.25	6.96	0.73	12.52	7.70	-11.97	-0.12	-5.20	4.13	13.81	8.25	3.92	21.90	14.39

Table 2. Porewater values for alkalinity (Alk., μM), dissolved inorganic carbon (DIC, μM), $\delta^{13}C$ (‰), $\delta^{18}O$ (‰), deuterium (δD, ‰) for all the bays of interest during each sampling event presented as the maximum, minimum, and average value. Overall average for each parameter is also provided. † Winter 2017 NB samples were collected from station 7 from Murgulet et al. (2018). ‡ Winter 2017 BB samples are from station 11 from Lopez et al. (2018).

		AB			NB†			UB			OB			LM			BB‡		
		Min.	Max.	Avg.	Min.	Max.	Avg.	Min.	Max.	Avg.	Min.	Max.	Avg.	Min.	Max.	Avg.	Min.	Max.	Avg.
December 2016 - January 2017	Alk.	3537	3586	3561	2621	2688	2654	--	--	--	4718	5251	4945	4431	5363	4897	9589	9616	9602
	DIC	3454	3627	3540	2444	2532	2488	--	--	--	4631	5382	4890	4202	5348	4775	9333	9389	9361
	$\delta^{13}C$	-8.13	-7.12	-7.62	-9.24	-3.25	-6.24	--	--	--	-5.92	-4.40	-5.20	-5.49	-5.46	-5.47	-8.76	-6.18	-7.47
	$\delta^{18}O$	-0.24	-0.22	-0.23	1.46	1.62	1.54	--	--	--	1.08	1.90	1.51	1.19	1.44	1.32	3.14	3.37	3.26
	δD	5.57	5.93	5.75	10.66	11.39	11.03	--	--	--	11.51	13.77	12.52	10.25	10.45	10.35	22.13	22.34	22.23
April - June 2017	Alk.	4514	4694	4601	2632	2708	2679	2709	2889	2799	2632	2632	2632	4565	5176	4871	3605	3758	3673
	DIC	4101	4316	4194	2481	2608	2544	2516	2698	2607	2594	2594	2594	4623	5257	4940	2066	3894	3185
	$\delta^{13}C$	-22.65	-9.37	-15.71	-3.13	-2.61	-2.91	-5.09	-3.84	-4.47	-7.90	-7.90	-7.90	-5.60	-5.24	-5.42	-6.59	-6.18	-6.32
	$\delta^{18}O$	-0.31	1.37	0.60	0.51	2.22	1.41	0.15	1.69	0.92	0.41	0.41	0.41	1.39	2.05	1.72	1.76	3.53	2.42
	δD	-3.36	10.54	2.80	4.40	16.05	9.71	2.70	11.03	6.86	-9.55	-9.55	-9.55	5.66	15.85	10.75	19.08	27.17	22.76
August - September 2017	Alk.	Goose Island State Park closed due to Hurricane Harvey damage.			2432	2463	2449	2636	2696	2661	--	--	--	4401	4822	4612	3685	3816	3750
	DIC				2322	2389	2351	2553	2635	2589	--	--	--	3812	4356	4084	3490	3595	3542
	$\delta^{13}C$				-3.85	-3.23	-3.58	-3.77	-3.46	-3.64	--	--	--	-5.93	-5.93	-5.93	-6.05	-5.90	-5.98
	$\delta^{18}O$				-0.42	-0.18	-0.32	0.65	1.20	1.01	--	--	--	0.52	0.78	0.65	-0.26	2.44	1.09
	δD				-6.67	-1.85	-3.77	14.59	18.08	15.92	--	--	--	7.73	9.02	8.37	12.29	15.42	13.85
December 2017 - January2018	Alk.	2728	2802	2765	2951	3203	3087	2621	2799	2712	2820	3078	2949	3512	4385	3949	3725	3799	3761
	DIC	2868	2983	2925	2948	3131	3041	2473	2783	2643	2743	2866	2804	3602	4286	3944	3301	3539	3410
	$\delta^{13}C$	-4.89	-4.83	-4.86	-6.00	-5.32	-5.67	-5.09	-3.33	-4.27	-5.37	-4.95	-5.16	-5.28	-4.80	-5.04	-6.31	-5.51	-5.99
	$\delta^{18}O$	-2.15	-1.16	-1.65	-0.05	1.28	0.42	-1.39	-0.13	-0.56	-2.07	1.42	-0.32	0.61	1.53	1.07	2.88	3.09	2.95
	δD	-9.83	-3.16	-6.49	-0.35	7.91	4.46	-2.09	3.81	1.76	0.34	8.29	4.32	8.27	11.50	9.89	17.25	17.73	17.45
Overall Avg.	Alk.	3593	3694	3642	2659	2765	2717	2655	2795	2724	3390	3653	3508	4227	4937	4582	5151	5247	5197
	DIC	3474	3642	3553	2549	2665	2606	2514	2705	2613	3323	3614	3430	4060	4811	4436	4547	5104	4875
	$\delta^{13}C$	-12	-7	-9	-6	-4	-5	-5	-4	-4	-6	-6	-6	-6	-5	-5	-7	-6	-6
	$\delta^{18}O$	-0.90	-0.01	-0.43	0.38	1.23	0.76	-0.20	0.92	0.46	-0.19	1.24	0.53	0.93	1.45	1.19	1.88	3.11	2.43
	δD	-2.54	4.44	0.69	2.01	8.37	5.36	5.06	10.97	8.18	0.77	4.17	2.43	7.98	11.71	9.84	17.69	20.66	19.07

Table 3. Surface water values for temperature (Temp., °C), dissolved oxygen (DO, mg/L), salinity (Sal), pH, and chlorophyll-α (Chl-α, µg/L) for all the bays of interest during each sampling event presented as the minimum, maximum, and average value. Overall average for each parameter is also provided. † Winter 2017 NB samples were collected from station 7 from Murgulet et al. (2018). ‡ Winter 2017 BB samples are from station 11 from Lopez et al. (2018).

		AB			NB†			UB			OB			LM			BB‡		
		Min.	Max.	Avg.	Min.	Max.	Avg.	Min.	Max.	Avg.	Min.	Max.	Avg.	Min.	Max.	Avg.	Min.	Max.	Avg.
December 2016 - January 2017	Temp	10.5	20.0	14.7	16.5	17.3	16.9	19.0	21.7	20.3	16.5	23.4	19.6	19.4	20.1	19.7	15.3	15.8	15.5
	DO	4.17	10.28	6.82	7.96	8.66	8.31	6.73	7.56	6.99	6.30	9.02	7.54	5.28	6.79	5.88	6.45	8.12	7.49
	Sal	19.50	19.97	19.79	27.71	27.96	27.81	27.51	28.78	28.29	28.69	31.60	31.11	33.49	33.82	33.68	44.50	44.59	44.55
	pH	7.62	8.34	8.01	8.02	8.10	8.05	7.97	8.13	8.05	7.92	8.19	8.03	7.84	7.90	7.86	8.10	8.16	8.14
	Chl-a	0.63	5.87	3.50	1.81	5.31	2.66	3.30	9.48	5.83	4.90	18.80	11.34	3.18	5.90	4.60	10.63	13.99	11.65
April - June 2017	Temp	22.4	28.6	24.4	23.7	27.9	25.9	28.5	33.5	31.7	25.9	32.6	30.4	22.4	25.1	23.9	25.4	30.0	27.5
	DO	5.00	11.27	7.36	6.17	8.07	6.99	3.67	7.36	6.18	5.37	9.15	7.07	6.09	7.65	6.93	4.11	9.14	6.47
	Sal	17.55	19.23	18.75	32.43	33.06	32.75	32.54	33.03	32.75	18.05	21.85	20.25	46.46	46.86	46.69	48.71	49.67	49.46
	pH	8.73	9.08	8.87	7.94	8.14	7.99	7.95	8.16	8.05	7.96	8.41	8.22	9.73	9.81	9.77	7.78	8.08	7.98
	Chl-a	6.94	24.75	11.95	4.67	9.98	7.09	7.61	15.15	10.82	11.42	50.43	28.34	9.07	12.22	10.63	2.90	33.97	22.85
August - September 2017	Temp	Goose Island State Park closed due to Hurricane Harvey damage.			25.3	28.1	26.4	28.4	35.9	31.4	28.1	34.2	30.6	27.3	29.5	28.4	27.0	30.2	28.8
	DO				3.96	5.29	4.50	1.60	5.21	3.46	1.59	6.81	4.12	3.63	5.89	4.67	2.63	5.87	4.12
	Sal				34.34	34.57	34.50	40.18	44.57	41.60	19.62	24.19	21.64	35.01	35.76	35.33	55.32	55.88	55.59
	pH				8.03	8.16	8.08	7.85	8.37	8.11	8.21	8.49	8.36	8.06	8.10	8.08	8.01	8.20	8.10
	Chl-a				9.80	22.92	13.24	0.34	27.40	11.58	17.88	71.15	30.98	0.93	3.81	2.60	14.91	22.57	19.05
December 2017 - January2018	Temp	16.1	16.6	16.4	12.0	15.6	14.1	14.1	16.4	15.4	11.1	19.5	14.9	17.3	19.2	18.2	11.6	12.1	11.9
	DO	1.02	2.13	1.56	1.67	3.41	2.02	2.06	8.61	4.21	2.71	9.29	3.60	1.84	2.03	1.90	1.67	4.26	2.64
	Sal	19.53	20.81	20.23	27.20	28.35	27.90	28.80	29.28	29.08	22.29	28.74	27.08	30.20	30.51	30.36	51.45	51.59	51.54
	pH	7.70	7.86	7.79	7.44	7.64	7.57	7.79	8.26	7.90	7.85	8.78	8.21	7.98	8.10	8.05	7.57	7.74	7.68
	Chl-a	3.03	9.33	5.85	0.51	2.15	1.11	0.79	9.60	2.95	1.99	16.13	5.53	1.53	3.76	2.39	0.63	8.23	4.60
Overall Avg.	Temp	16.3	21.7	18.5	19.4	22.2	20.8	22.5	26.9	24.7	20.4	27.4	23.9	21.6	23.5	22.5	19.8	22.0	20.9
	DO	3.40	7.89	5.24	4.94	6.36	5.45	3.52	7.19	5.21	3.99	8.57	5.58	4.21	5.59	4.84	3.72	6.85	5.18
	Sal	18.9	20.0	19.6	30.4	31.0	30.7	32.3	33.9	32.9	22.2	26.6	25.0	36.3	36.7	36.5	50.0	50.4	50.3
	pH	8.02	8.43	8.22	7.86	8.01	7.92	7.89	8.23	8.03	7.99	8.47	8.20	8.40	8.48	8.44	7.87	8.05	7.98
	Chl-a	3.53	13.32	7.10	4.20	10.09	6.02	3.01	15.41	7.79	9.05	39.13	19.05	3.68	6.42	5.05	7.27	19.69	14.54

Table 4. Porewater values for temperature (Temp., °C), dissolved oxygen (DO, mg/L), salinity (Sal), and pH for all the bays of interest during each sampling event presented as the minimum, maximum, and average value. Overall average for each parameter is also provided. † Winter 2017 NB samples were collected from station 7 from Murgulet et al. (2018). ‡ Winter 2017 BB samples are from station 11 from Lopez et al. (2018).

		AB			NB†			UB			OB			LM			BB‡		
		Min.	Max.	Avg.	Min.	Max.	Avg.	Min.	Max.	Avg.	Min.	Max.	Avg.	Min.	Max.	Avg.	Min.	Max.	Avg.
December 2016 - January 2017	Temp	15.0	17.9	16.5	17.6	18.7	18.2				16.6	18.9	17.7	18.3	19.9	19.1	22.9	23.2	23.1
	DO	0.74	1.80	1.27	0.74	0.82	0.78				2.10	4.65	3.66	0.75	0.92	0.84			
	Sal	18.91	18.96	18.94	27.75	27.97	27.86				28.16	31.07	30.04	35.08	36.79	35.94	56.39	56.47	56.43
	pH	7.61	7.67	7.64	7.60	7.71	7.66				7.26	7.46	7.35	7.12	7.48	7.30	6.67	6.67	6.67
April - June 2017	Temp	22.9	24.2	23.7	23.2	27.7	25.2	30.6	31.3	31.0			33.3	24.7	25.0	24.9	24.4	29.7	27.3
	DO	0.80	2.33	1.60	1.36	2.48	1.94	0.46	1.78	1.12			1.55	0.71	1.32	1.02	0.58	1.79	1.33
	Sal	19.53	19.85	19.68	32.80	33.06	32.91	30.59	32.13	31.36			19.84	42.71	43.07	42.89	45.29	46.00	45.68
	pH	7.94	8.09	8.02	7.58	7.60	7.59	7.74	7.84	7.79			7.51	8.45	8.60	8.53	7.27	7.34	7.30
August - September 2017	Temp	Goose Island State Park closed due to Hurricane Harvey damage.			23.9	28.3	25.5	29.5	31.2	30.6				28.6	29.5	29.1	28.2	28.9	28.6
	DO				1.22	4.13	2.52	1.42	7.08	3.47				4.10	4.10	4.10	0.68	1.81	1.25
	Sal				33.86	34.30	34.02	0.33	40.84	27.20				44.17	45.58	44.88	55.91	56.14	56.03
	pH				7.39	7.60	7.49	7.51	7.85	7.63				7.10	7.19	7.15	7.29	7.31	7.30
December 2017 - January2018	Temp	16.5	19.0	17.9	12.7	14.6	13.7	14.1	17.6	15.9	11.6	12.9	12.3	19.0	19.0	19.0	11.7	14.1	13.2
	DO	0.85	1.56	1.10	0.67	1.45	0.96	1.58	3.33	2.46	2.51	3.23	2.87	0.30	0.30	0.30	0.62	1.49	0.97
	Sal	18.58	20.99	19.23	27.51	27.81	27.68	29.31	29.72	29.46	28.42	29.50	28.96	37.04	39.63	38.34	53.23	54.00	53.70
	pH	7.53	7.77	7.67	7.13	7.22	7.17	7.58	7.62	7.60	7.53	7.61	7.57	7.32	7.37	7.35	6.98	7.15	7.06
Overall Avg.	Temp	18.1	20.4	19.3	19.4	22.3	20.6	24.7	26.7	25.8	14.1	15.9	21.1	22.7	23.4	23.0	21.8	24.0	23.0
	DO	0.80	1.90	1.32	1.00	2.22	1.55	1.15	4.06	2.35	2.31	3.94	2.69	1.47	1.66	1.56	0.63	1.70	1.18
	Sal	19.01	19.93	19.28	30.48	30.79	30.62	20.08	34.23	29.34	28.29	30.29	26.28	39.75	41.27	40.51	52.71	53.15	52.96
	pH	7.69	7.84	7.78	7.43	7.53	7.48	7.61	7.77	7.67	7.40	7.54	7.48	7.50	7.66	7.58	7.05	7.12	7.08

$\delta^{18}O$ and $\delta^{15}N$ of Nitrate

Nitrogen and oxygen isotopes of nitrate ratio abundances have been used successfully for tracing inputs of nitrogen to surface and subsurface reservoirs. In this study, isotope measurements were conducted using the denitrifier method (Casciotti et al., 2002) which requires a minimum nitrate concentration of 0.7 µM of nitrate. A subset of samples met the criteria and where thus, analyzed for these isotopes. An entire time series event from Oso Bay exhibited large enough concentrations in surface water and are included in the figure below **Figure 3**. Some samples from Baffin Bay were also analyzed. Based on a suite of measurements done on other data sets available from parallel, or former studies, were used herein to evaluate the potential sources of nitrogen to all bays.

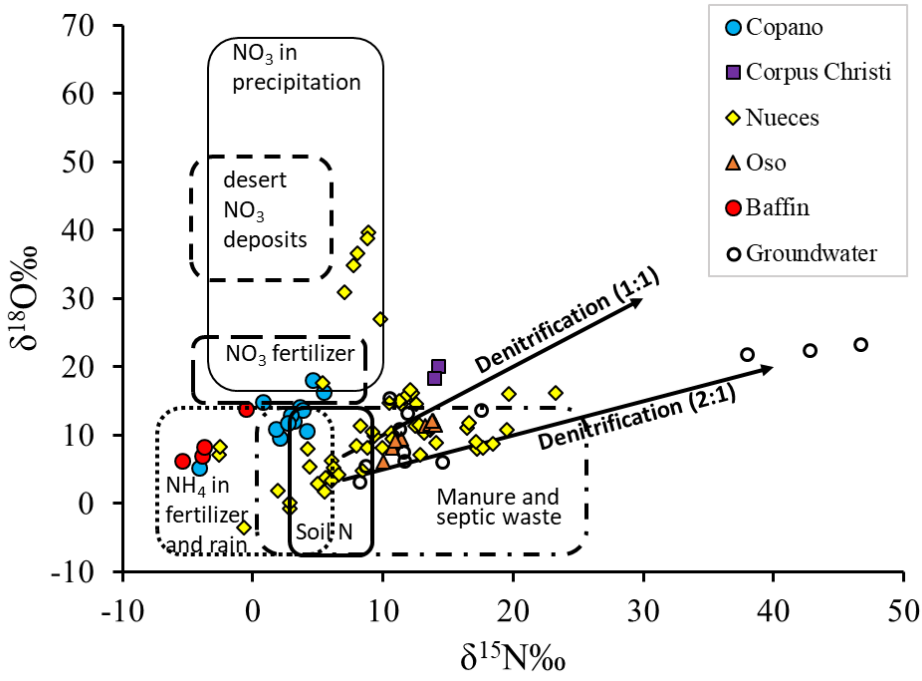

Figure 3. Cross-correlation of $\delta^{18}O$ and $\delta^{15}N$ of NO_3 including potential source regions and denitrification pathways from Kendall and McDonnell (2012).

Using the typical isotope source signatures from Kendall and McDonnell (2012), and based on a limited data sample size, sources of nitrate to Baffin Bay (in Laguna Salada) and Copano Bay (part of Aransas Bay system) seem to be associated with fertilizer application. Some denitrification and or mixing of different fertilizer types (i.e., nitrate and ammonium fertilizer) may have also occurred. Oso Bay samples indicate a potential septic and manure waste, potentially from wildlife and/or pet waste. The monitoring station in Oso Bay was located at the South Bay park, thus the potential for animal waste input into the bay, through runoff and subsurface transport.

The Nueces Bay samples are representative of a few seasons. The group of samples plotting within the nitrate in precipitation field were collected before the 2015 flood, at the end of a five-year drought period. A significant decline in the water table due to almost absent precipitation and thus, recharge, likely limited shallow groundwater input to the bay. This, together with absent surface and riverine inputs, lead to reduced terrestrial inputs of nitrogen. All other seasons indicate a variety of nitrogen sources spanning from ammonium fertilizer to septic and manure. Denitrification also seems to play an important role as a majority of data plot along the denitrification lines. Two samples from Corpus Christi Bay collected also towards the end of the five-year drought show a potential influence of both atmospheric nitrogen and manure/septic, although denitrification may have altered a possibly more dominant soil nitrogen source.

Oxygen and Hydrogen Stable Isotopes

A common application of stable isotopes in many areas is to ascertain the apportioning of sources within a mixture (Bowen et al. 2018). The stable isotopes of oxygen and hydrogen in water are important tracers of the global, regional, and local hydrologic cycle. The importance of

these isotopes as tracers in water management has been long recognized by the International Atomic Energy Agency (IAEA) which maintains a Global Network of Isotopes in Precipitation (GNIP) providing the isotopic signatures of precipitation worldwide since 1961.

In this study, surface water δD and $\delta^{18}O$ ratio abundances ranged from –4.2 ‰ and –32.2‰, respectively, in Oso Bay in summer 2016 to 4.3‰ to 29.9‰, respectively, in Laguna Madre in spring 2017. Oso Bay also exhibited the most depleted signatures of all bays in spring 2016. Seasonal averages indicate that the most depleted δD and $\delta^{18}O$ ratio abundances occurred in Oso Bay while the most enriched in in Baffin Bay (**Table 1**). In winter 2017 each bay showed occurrences of more depleted signatures as oppose to the other seasons. As indicated in the previous section, Aransas Bay exhibited the lowest salinity. The most depleted δD and $\delta^{18}O$ ratio abundances thus, are not linked with the lowest salinity when all the bays are considered. However, the most enriched isotopic abundances are found in Baffin Bay, the most saline of all bays. It should be noted that, freshwater inflows are expected to bring more depleted abundances of the δD and $\delta^{18}O$ isotopes (Henderson and Shuman 2010).

As oppose to surface water, porewater abundances mimic closely the salinity. Thus, the most depleted δD and $\delta^{18}O$ were measured in porewaters from Aransas Bay (all seasons average: -0.9 ‰ and -2.5‰, respectively) while the most enriched δD and $\delta^{18}O$ occurred in Baffin Bay (all seasons average: 2.4‰ and 19.1‰, respectively). University Beach and Oso Bay follow with more enriched abundances when compared to Aransas Bay, but slightly more depleted than Laguna Madre. Laguna Madre, although on the more enriched end, is in average more depleted than Baffin Bay. This indicates the greater effect of evaporation and limited freshwater input the southern Upper Laguna Madre estuary.

As mentioned above, the change or degree of isotopic enrichment in porewater is observed to follow a similar pattern as the salinity (**Table 2**; **Table 4**). One obvious exception is Nueces Bay in summer, when the most depleted abundances were measured in porewater. Nevertheless, Aransas Bay and Oso Bay porewater is not available for this event. Although, salinity slightly increased from spring, the δD and $\delta^{18}O$ decreased from a spring average of 1.4 ‰ and 9.7‰, respectively, to -0.3 ‰ and -3.8‰, respectively. The summer event at all locations but University Beach took place after Hurricane Harvey. Nueces Bay was sampled at a short time after the hurricane which delivered more rain to the northern bays/watersheds. In fact, there was very little rain in the Baffin Bay area. Aquifer recharge from rain as well as the significant drop in bay water levels observed during Harvey may explain the more depleted porewater isotope signatures. Though, salinity levels are still very high.

Enriched δD and $\delta^{18}O$ ratios are generally correlated with lower amounts of rainfall and higher evaporation rates (Katz et al. 1997) which are the result of both high wind and high temperature conditions. δD and $\delta^{18}O$ abundances are much more depleted in groundwater around this area with samples collected in May 2015 as part of this study ranging from –26.6 ‰ to -7.3‰ (average –21.2 ± 1‰) and –4.96 ‰ to –2.0 ‰ (average –4.0 ± 1), respectively. Bighash and Murgulet (2015) reported more enriched and variable δD and $\delta^{18}O$ signatures in shallow wells in close proximity of this study's Oso Bay sampling station. Average δD and $\delta^{18}O$ for groundwater samples collected as part of their study in summer 2012 (-16.8 ± 1‰ and -0.9 ± 0.1‰, respectively) and spring 2013 (-9.5 ± 1‰ and -1.8 ± 0.1‰, respectively) show a change towards more enriched δD ratios and slightly depleted $\delta^{18}O$ for the 2013 dry spring season. This clearly shows that shallow groundwater isotope signature could be variable as dependent on recharge conditions. This conditions likely changed since the end of the long-term droughts in

summer 2015 as spring, fall and winter seasons have been wet, likely leading to freshening and isotope depletion in the shallow groundwater and groundwater discharging to the bays. Two shallow wells located across from the University Beach location have been sampled a few times during the study period. The δD and $\delta^{18}O$ signatures observed during our study period vary dependent largely on the precipitation depths, thus a climatic response is observed and is expected to reflect in the porewater and surface water signatures as well.

All locations show a clear mixing pattern between surface water and porewater δD and $\delta^{18}O$ signatures. This is an indication that surface water and porewater are mixing, with larger degrees where porewaters have signatures more like surface water.

Spatial-temporal Distribution of Phytoplankton and Nutrients

The maximum chl-α concentrations were consistently lower than 16 µg/L across all bays during the winter seasons. The average concentrations ranged between 2.7 and 11.7 µg/L in winter 2017 and between 1.1 and 5.9 µg/L in winter 2018. The concentrations increase by spring 2017, particularly in Oso and Baffin bays with maximums of 50.4 and 34 µg/L, respectively. Nueces Bay and University Beach are increasing only slightly from spring to summer (average spring: 7.1 and 10.8 µg/L, respectively; average summer: 13.2 and 11.6 µg/L, respectively). However, maximum concentrations observed in Oso Bay are significantly higher in summer 2017 when compared to spring 2017 (maximum spring and summer: 50.4 and 71.2 µg/L). Oso and Baffin bays are consistently the highest across all seasons, except for winter 2018 when Aransas Bay is also higher (**Table 3; Figure 4**). In Laguna Madre, chl-α concentrations increase from winter to spring 2017 but decrease by approximately five times to summer 2017 and winter 2018.

The observed late spring and summer increase in chl-α and lower concentrations in winter are a seasonal characteristic in many coastal systems, associated with physical environmental factors. Both light and temperature have been found to be associated with primary productivity in other Texas estuaries (Longley et al. 1994). Nevertheless, the fluctuation in the inflow of nutrients is another factor to consider.

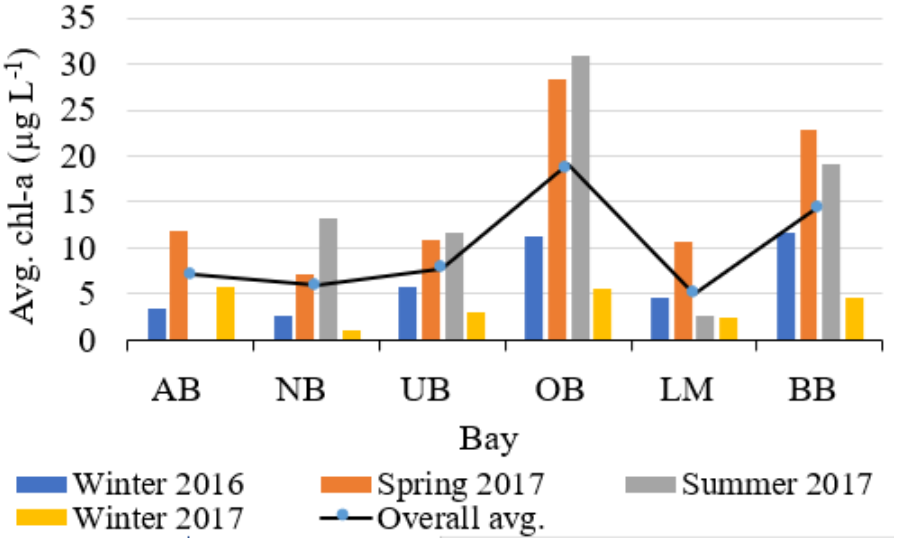

Figure 4. Seasonal average chl-α concentrations by bay.

DON was calculated, for surface water only, as the difference between TN and dissolved inorganic nitrogen (DIN: sum of nitrate, nitrite and ammonium). DON concentrations are in average the lowest in Aransas Bay and the highest in Baffin Bay, with a gradual increase in concentration along the hydroclimatic gradient (**Figure 5A**). The majority (in average ~90%) of TN in all systems consists of DON. While DON follows an increasing gradient from north to south, nitrate, nitrite and ammonium (i.e. DIN) do not show a steady increase from Aransas Bay to Baffin Bay (**Figure 5B, C, D**). While most nitrate concentrations throughout the bays and seasons are consistently below 2.5 µM, Oso Bay exhibits much larger concentrations during the two winter seasons (i.e. max: 72.5 and 139.6 µM in winter 2017 and 2018, respectively). These were also accompanied by the highest nitrite levels (i.e. max: 1.4 and 1.3 µM in winter 2017 and

2018, respectively), although not as different than the rest of the bays (**Figure 5C, D**). The second largest nitrite concentrations occurred in Baffin Bay, also during the winter events (i.e. max: 1.1 and 0.6 μM in winter 2017 and 2018, respectively).

Ammonium concentrations are less than 10 μM across all bays and seasons. Winter 2017 ammonium concentrations are the largest in Aransas, Oso, and Baffin bays and University Beach while Nueces Bay and Laguna Madre are the lowest. Spring 2017 ammonium levels are also more elevated that in summer 2017 (**Figure 5B**). The highest concentrations, however, were measured in summer 2017 and winter 2018 in Baffin Bay which also exhibited the highest all seasons average concentration. Oso Bay has the second highest overall average of ammonium. Ammonium is typically thought to be a preferred nitrogen source for phytoplankton (Dortch 1990), so the preferential uptake of ammonium may be heightened in areas of severe N-limitation as seen in the northern two bays (i.e., Aransas and Nueces bays).

TN, which includes the DON and DIN, follows a very similar trend with the DON and TOC, with very minor seasonal differences in Oso Bay (**Figure 5E, H**). The largest average concentrations were measured in Baffin Bay (127.1 μM) followed by Oso Bay (89.8 μM). The TN concentration increases across the hydroclimatic gradient, with the lowest concentrations in Aransas and Nueces bays (**Figure 5E**).

Phosphate and silica do not follow the increasing concentration gradient from north to south but, as with nitrate, exhibit higher concentrations in Oso Bay (i.e., average phosphate and silica: 6.1 and 93.6 μM, respectively). In average, phosphate and silica concentrations decrease slightly from Aransas Bay to Nueces to University Beach, increas in Oso Bay, decrease in Laguna Madre and increase again in Baffin Bay. While the highest phosphate concentration

occurs in Oso Bay, the highest silica concentrations (ranging from 177.4 in winter 2017 to 186.4 in winter 2018) were measured in Baffin Bay across all seasons (**Figure 5F, G**).

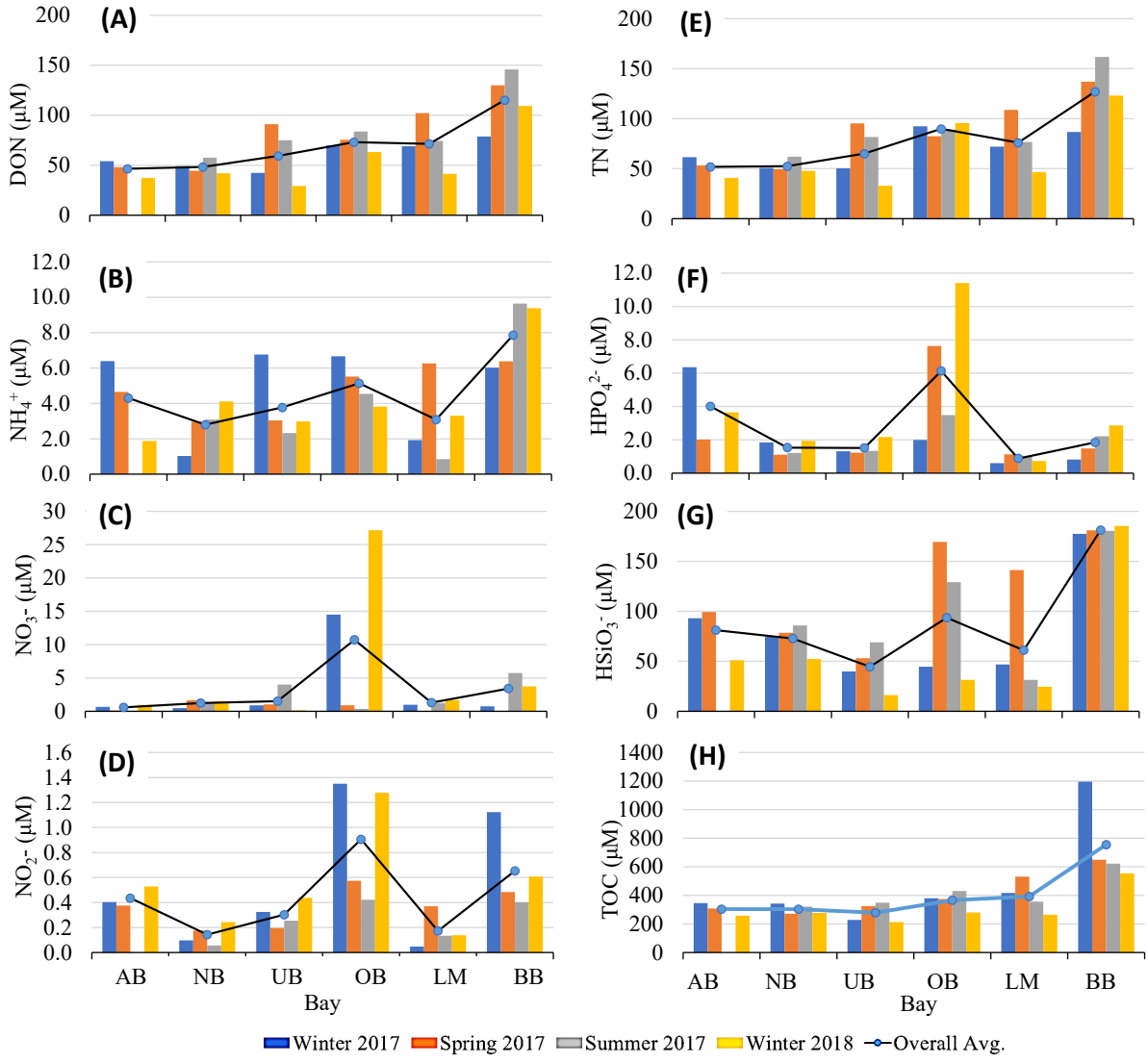

Figure 5. Seasonal changes in surface water nutrient concentrations across all bays.

TOC concentrations are similar among the Aransas and Nueces bays and University Beach, and consistently below 400 µM) and increase gradually from Oso Bay (366.2 and 392.4 µM, respectively) towards Baffin Bay (755.4 µM) (**Figure 5H**). A significantly higher TOC concentration was measured in Baffin Bay in winter 2017 (1196.4 µM compared to the all seasons average 755.4 µM). No seasonal trend is observed except for three instances of larger

TOC concentrations in winter 2017 for Aransas and Nueces Bay and, as mentioned above, Baffin Bay.

Overall, average nutrient concentrations in porewater (**Figure 6**) follow the same trend across the bays as with surface water (**Figure 5**). Porewater concentrations of most nutrients were higher than in the water column (silicate, TN, nitrate, phosphate, ammonium). This difference was most pronounced for ammonium, with porewater samples having 10 to 100x higher concentrations than the water column (**Figure 6C**). Overall, the highest ammonium concentrations were measured in Aransas, Oso, and Baffin bays. These bays, in particular Baffin Bay, also exhibit some of the most elevated ammonium surface water concentrations (**Figure 5B; Figure 6C**).

Nitrate and nitrite concentrations are only slightly more elevated than surface water, except for Oso Bay in winter 2017 when porewater concentrations are much larger (average nitrate and nitrite winter 2017: 182.7 and 9.4 μM, respectively) (**Table 6**). Concentrations of nitrate are also higher in winter 2018, in both Oso and Baffin Bays (average: 14.1 and 18.0 μM, respectively). Interestingly, for the same seasons at these locations, surface water has also the highest nitrate and nitrite concentrations. This suggests that porewater may be an intermittently important source for inorganic nutrients to these bays, and in particular to Oso and Baffin bays. The potential importance of porewater as a source for organic nutrient inputs to the system cannot be ruled out either, although DON concentrations in porewater could not be determined in this study. Unlike the other nutrients measured, TOC concentrations were slightly more elevated in the water column, but they follow a very similar trend as surface water, with increasing concentrations from north to south.

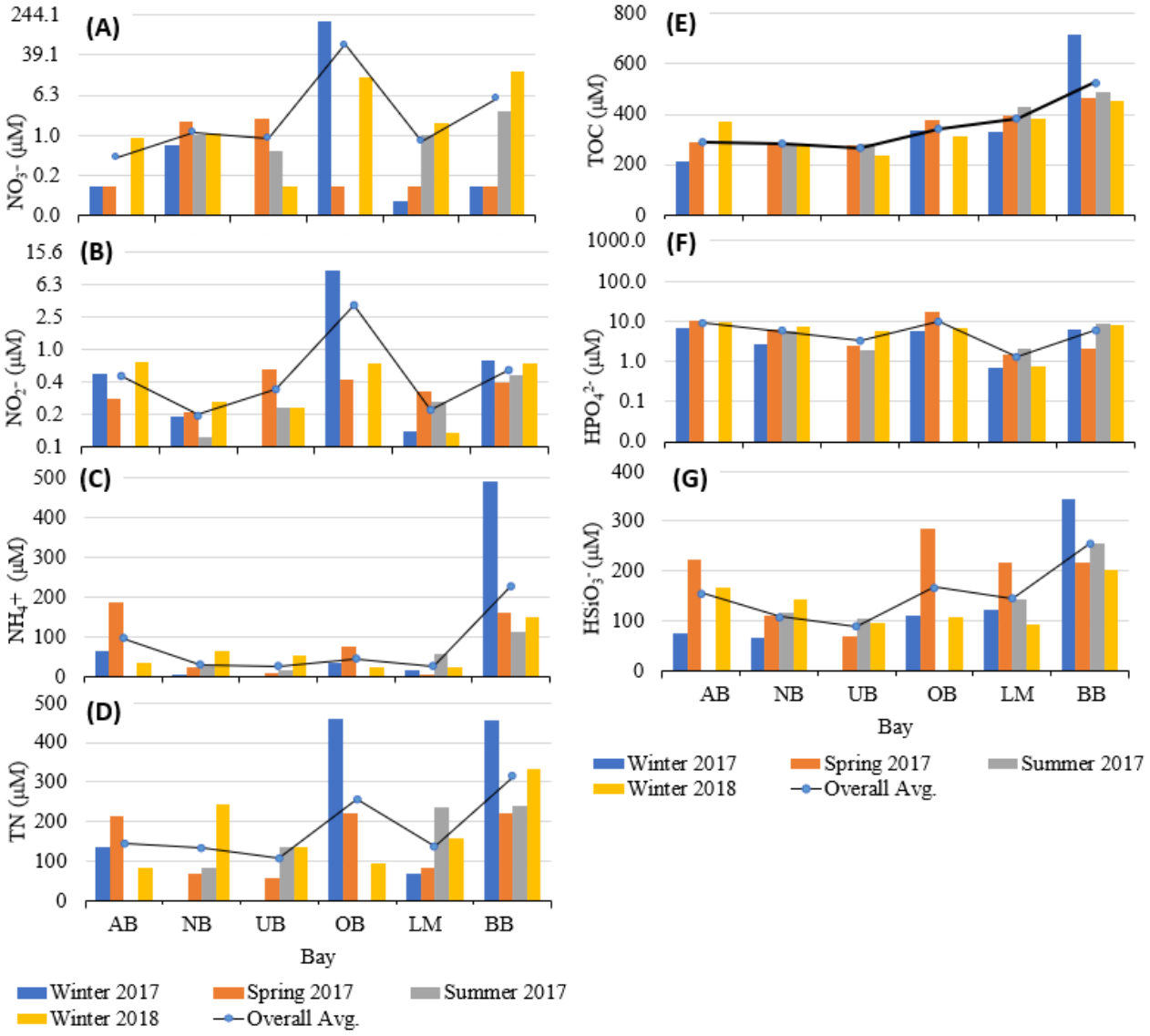

Figure 6. Seasonal changes in porewater nutrient concentrations across all bays.

Table 5. Surface water nutrients including nitrate (NO_3), nitrite (NO_2), ammonium (NH_4), orthophosphate (HPO_4), silicate ($HSiO_3$), urea, total organic carbon (TOC), and total nitrogen (TN) presented in $\mu mol \cdot L^{-1}$ (μM) for bays of interest. Values below method detection limit are indicated by BDL. † Winter 2017 NB samples were collected from station 7 from Murgulet et al. (2018). ‡ Winter 2017 BB samples are from station 11 from Lopez et al. (2018).

		AB			NB†			UB			OB			LM			BB‡		
		Min.	Max.	Avg.	Min.	Max.	Avg.	Min.	Max.	Avg.	Min.	Max.	Avg.	Min.	Max.	Avg.	Min.	Max.	Avg.
December 2016 - January 2017	NO_3	BDL	3.6	0.7	BDL	2.3	0.5	BDL	2.7	0.9	4.0	72.5	14.5	BDL	2.5	1.0	0.1	1.2	0.7
	NO_2	0.2	0.6	0.4	BDL	0.3	0.1	0.1	0.7	0.3	0.8	3.1	1.4	BDL	0.1	0.0	1.1	1.2	1.1
	NH_4	3.2	8.4	6.4	BDL	2.9	1.0	4.3	10.1	6.8	1.5	9.8	6.7	1.1	3.4	1.9	4.2	14.5	6.0
	HPO_4	3.7	10.5	6.4	1.3	3.3	1.8	0.8	2.2	1.3	1.0	6.0	2.0	0.4	0.8	0.6	0.7	0.9	0.8
	$HSiO_3$	66.8	114.3	93.1	65.9	86.2	74.4	29.1	51.4	39.9	35.7	56.5	44.6	41.3	58.6	46.8	174.6	182.1	177.4
	Urea	1.5	2.2	1.7	0.5	1.3	0.8	0.3	1.4	0.7	0.5	1.5	1.0	0.4	0.9	0.7	1.2	2.4	2.0
	TOC	250.3	404.2	345.9	336.9	350.5	342.8	168.8	265.4	228.1	301.4	699.3	379.5	380.2	440.4	416.9	1060.7	1468.7	1196.4
	DON	46.8	58.6	54.0	46.1	49.2	49.1	28.3	59.3	42.3	53.1	171.5	69.8	63.4	72.6	69.0	74.7	77.9	78.8
	TN	50.2	71.2	61.5	46.1	54.7	50.7	32.7	72.8	50.3	59.5	256.9	92.3	64.5	78.6	72.0	80.1	94.7	86.7
April - June 2017	NO_3	BDL	1.4	0.1	0.8	3.4	1.7	0.2	2.4	1.0	BDL	1.8	0.9	BDL	BDL	BDL	BDL	BDL	BDL
	NO_2	0.3	0.4	0.4	0.1	0.4	0.2	0.1	0.4	0.2	0.4	0.9	0.6	0.2	0.5	0.4	0.3	0.8	0.5
	NH_4	3.2	6.9	4.7	2.4	4.2	3.0	2.2	4.6	3.0	3.9	9.0	5.5	2.6	7.9	6.3	4.7	8.7	6.4
	HPO_4	1.6	2.8	2.0	0.6	2.4	1.1	1.0	1.9	1.2	6.5	9.2	7.6	0.9	1.8	1.1	1.0	1.9	1.5
	$HSiO_3$	82.3	122.3	99.3	58.4	101.9	78.5	44.0	64.3	53.0	117.3	201.8	169.4	130.2	158.3	141.3	165.9	199.1	181.0
	Urea	1.0	1.5	1.2	0.2	1.2	0.5	0.4	1.0	0.6	1.2	2.0	1.6	1.7	2.0	1.8	1.1	1.8	1.6
	TOC	237.1	514.4	307.9	231.6	306.3	271.6	261.2	549.9	324.9	353.2	387.5	374.1	483.1	558.6	531.4	582.6	722.2	649.2
	DON	40.8	59.6	48.2	40.4	45.4	44.6	50.9	337.3	91.0	73.6	77.9	75.5	100.7	106.6	102.2	113.3	150.0	130.0
	TN	44.2	68.4	53.3	43.7	53.5	49.4	53.3	344.6	95.3	78.0	89.6	82.4	103.5	115.0	108.8	118.2	159.6	136.9
August - September 2017	NO_3	Goose Island State Park closed due to Hurricane Harvey damage.			0.9	2.5	1.3	BDL	42.9	4.0	BDL	1.9	0.4	0.6	2.2	1.2	1.5	29.9	5.7
	NO_2				0.0	0.1	0.1	0.1	0.4	0.3	0.3	0.6	0.4	BDL	0.4	0.1	0.4	0.5	0.4
	NH_4				2.1	5.6	3.1	1.5	3.2	2.3	3.5	6.8	4.5	0.4	1.9	0.9	5.2	21.2	9.6
	HPO_4				0.7	3.7	1.2	0.6	2.6	1.3	2.5	4.4	3.5	0.1	2.6	1.0	1.0	3.4	2.2
	$HSiO_3$				61.4	108.7	85.9	46.0	77.8	68.9	95.4	153.7	129.1	22.8	36.6	31.4	146.6	220.7	180.5
	Urea				0.1	0.3	0.2	0.4	1.1	0.6	0.8	1.6	1.2	0.3	1.3	0.5	1.3	2.4	2.0
	TOC				284.5	353.2	321.1	308.2	431.8	348.4	292.7	488.8	430.6	320.6	388.2	356.5	575.9	652.5	621.7
	DON				52.5	59.4	57.5	58.0	91.4	75.0	66.2	89.7	83.7	67.2	79.3	74.4	124.1	154.8	145.9
	TN				55.5	67.6	61.9	59.6	137.8	81.6	70.0	98.9	89.1	68.2	83.8	76.6	131.1	206.3	161.7
December 2017 - January2018	NO_3	0.7	1.6	1.0	0.7	3.1	1.5	BDL	0.5	0.1	BDL	139.6	27.2	1.3	2.0	1.7	2.2	7.9	3.7
	NO_2	0.4	0.8	0.5	0.2	0.3	0.2	0.2	0.6	0.4	0.3	3.6	1.3	0.1	0.2	0.1	0.6	0.7	0.6
	NH_4	1.0	3.3	1.9	3.0	5.2	4.1	1.6	4.1	3.0	2.3	5.4	3.8	2.7	4.1	3.3	3.8	26.5	9.4
	HPO_4	2.3	7.3	3.6	0.9	3.8	1.9	1.1	3.3	2.2	4.1	42.6	11.4	0.5	1.2	0.7	0.8	4.7	2.9
	$HSiO_3$	34.8	73.8	51.0	32.1	82.7	52.3	12.2	20.2	16.2	7.5	103.1	31.4	18.8	30.2	24.6	160.5	202.6	185.4
	Urea	1.7	3.2	2.1	0.6	0.8	0.7	0.6	1.7	1.2	0.6	1.5	1.0	0.4	0.8	0.6	1.9	4.7	3.1
	TOC	213.9	316.9	258.0	239.8	308.5	277.0	171.2	241.6	212.8	218.1	349.3	280.6	255.6	270.0	265.0	487.4	601.5	554.4
	DON	32.3	43.4	37.3	36.8	47.6	41.9	24.9	37.0	29.3	45.0	128.7	63.2	35.7	50.0	41.3	104.6	101.0	109.3
	TN	34.5	49.0	40.7	40.7	56.1	47.8	26.7	42.3	32.9	47.7	277.3	95.5	39.8	56.2	46.4	111.2	136.1	123.0

Table 6. Porewater nutrients including nitrate (NO_3), nitrite (NO_2), ammonium (NH_4), orthophosphate (HPO_4), silicate ($HSiO_3$), urea, total organic carbon (TOC), and total nitrogen (TN) presented in $\mu mol \cdot L^{-1}$ (μM) for bays of interest. Values below method detection limit are indicated by italics. † Winter 2017 NB samples were collected from station 7 from Murgulet et al. (2018). ‡ Winter 2017 BB samples are from station 11 from Lopez et al. (2018).

		AB			NB†			UB			OB			LM			BB‡		
		Min.	Max.	Avg.	Min.	Max.	Avg.	Min.	Max.	Avg.	Min.	Max.	Avg.	Min.	Max.	Avg.	Min.	Max.	Avg.
December 2016 - January 2017	NO_3	*0.10*	*0.10*	*0.10*	0.24	1.05	0.65				120.28	270.45	182.65	*0.10*	0.17	0.05	*0.10*	*0.10*	*0.10*
	NO_2	0.36	0.64	0.50	*0.01*	0.47	0.15				4.80	12.79	9.39	*0.01*	0.17	0.10	0.69	0.76	0.74
	NH_4	49.03	85.50	66.51	5.67	10.81	7.41				17.77	46.27	33.66	3.47	30.52	16.87	481.27	495.80	488.18
	HPO_4	5.88	7.66	6.78	2.55	2.94	2.69				2.38	7.58	5.58	0.48	0.91	0.69	5.05	6.87	6.19
	$HSiO_3$	47.89	96.52	74.85	46.11	75.77	65.75				98.17	125.52	111.93	109.99	131.00	121.72	257.68	378.47	345.23
	Urea	1.29	2.25	1.67	0.07	2.71	1.07				0.65	1.13	0.93	0.44	0.56	0.47	2.22	2.91	2.54
	TOC	173.65	248.59	211.12							303.43	372.25	334.92	280.19	383.77	331.98	596.37	823.25	715.07
	TN	106.32	169.68	138.00							367.25	587.26	459.43	42.60	98.71	70.65	438.64	469.48	456.24
April - June 2017	NO_3	*0.10*	*0.10*	*0.10*	1.36	2.81	1.88	0.89	3.30	2.09			*0.10*	*0.10*	*0.10*	*0.10*	*0.10*	*0.10*	*0.10*
	NO_2	0.12	0.35	0.25	0.10	0.31	0.17	0.46	0.71	0.58			0.44	0.29	0.36	0.32	0.36	0.44	0.40
	NH_4	172.54	202.32	188.36	13.00	36.28	25.53	9.48	9.59	9.53			76.16	4.47	7.76	6.32	154.59	173.31	159.92
	HPO_4	9.06	10.54	9.89	3.29	8.63	6.39	2.22	2.83	2.53			17.63	1.32	1.60	1.45	1.94	2.10	2.04
	$HSiO_3$	210.04	248.27	223.93	101.73	120.32	110.97	69.28	70.27	69.77			283.89	195.49	238.82	217.68	198.38	235.43	218.34
	Urea	0.51	0.76	0.60	0.28	0.50	0.38	0.77	1.03	0.90			1.33	1.09	1.25	1.17	1.13	1.31	1.25
	TOC	260.12	336.63	286.07	231.73	337.71	280.52	254.82	298.36	276.59			377.86	382.84	403.52	393.18	447.86	471.86	463.14
	TN	206.48	220.13	213.01	56.38	84.73	69.09	52.84	63.09	57.97			220.00	73.72	91.79	82.76	205.13	238.68	223.24
August - September 2017	NO_3	Goose Island State Park closed due to Hurricane Harvey damage.			0.99	1.05	1.03	*0.10*	1.72	0.49				0.97	1.13	1.05	2.01	3.87	2.94
	NO_2				0.07	0.10	0.09	0.16	0.28	0.20				0.22	0.24	0.23	0.39	0.61	0.50
	NH_4				25.55	31.59	27.58	13.19	19.87	16.06				15.47	103.04	59.25	101.00	125.00	113.00
	HPO_4				3.04	7.34	5.55	1.66	2.02	1.88				1.99	2.26	2.13	7.56	9.26	8.41
	$HSiO_3$				78.33	167.23	115.82	97.15	113.50	104.51				133.56	153.98	143.77	238.87	271.48	255.17
	Urea				0.18	0.90	0.42	0.45	1.18	0.72				0.53	0.64	0.59	1.09	1.17	1.13
	TOC				273.24	291.96	281.13	274.77	287.14	280.00				407.44	451.13	429.29	484.48	490.65	487.56
	TN				76.90	96.88	83.83	127.76	146.01	135.15				78.86	395.82	237.34	222.12	262.32	242.22
December 2017 - January2018	NO_3	0.71	1.06	0.89	0.98	1.21	1.07	*0.10*	*0.10*	*0.10*	5.04	23.17	14.10	1.67	1.86	1.76	2.17	33.50	17.98
	NO_2	0.70	0.73	0.72	0.21	0.25	0.23	0.14	0.29	0.19	0.40	0.97	0.68	0.06	0.14	0.10	0.46	0.91	0.68
	NH_4	32.20	36.02	34.11	47.60	83.18	65.36	27.92	74.31	54.32	21.63	29.47	25.55	24.08	24.31	24.20	129.01	167.33	150.15
	HPO_4	7.92	11.23	9.58	6.52	8.07	7.19	4.13	6.22	5.48	4.27	9.66	6.97	0.63	0.92	0.78	5.58	10.22	7.80
	$HSiO_3$	167.04	167.77	167.40	139.71	146.56	142.34	71.03	113.72	95.81	97.61	118.88	108.24	84.09	101.82	92.96	191.89	211.72	202.64
	Urea	1.71	1.75	1.73	0.53	0.48	0.56	0.60	0.94	0.72	0.57	0.64	0.61	0.16	0.34	0.25	1.71	2.53	2.09
	TOC	261.85	484.22	373.03	275.35	269.93	284.91	216.43	264.84	237.36	275.49	349.58	312.53	369.01	396.90	382.96	439.36	459.54	450.65
	TN	84.37	85.35	84.86	192.47	100.98	245.93	91.00	158.82	136.01	92.87	99.58	96.22	97.17	221.15	159.16	318.77	342.86	332.31

Radiogenic Isotopes and Submarine Groundwater Discharge

Surface Water Radium Activities

Activities of ^{226}Ra were in average 557.3±55.7 dpm·m^{-3} across all seasons for all the bays. The highest average ^{226}Ra surface water activity was measured in spring 2017 ($\bar{x}$: 1623.7±162.4 dpm·m^{-3}) in Baffin Bay, while the lowest occurred in winter 2018 ($\bar{x}$: 186.0 ±18.6 dpm·m^{-3}), in Laguna Madre followed by winter 2017 ($\bar{x}$: 222.5±22.3 dpm·m^{-3}; n=10), at the University Beach (**Figure 7A**; **Table 7**)**.** The highest average activities of all four seasons were found in Baffin Bay ($\bar{x}$: 1032.3±103.2 dpm·m^{-3}) while the lowest at University Beach ($\bar{x}$: 283.1±28.3 dpm·m^{-3}). The lowest activities were almost consistently measured at the University Brach followed by Laguna Madre and Oso Bay. Across all bays, the lowest average ^{226}Ra ($\bar{x}$: 409.9±41 dpm·m^{-3}) was measured in winter 2018 followed by winter 2017 ($\bar{x}$: 474.6±47.5 dpm·m^{-3}). The highest average activity across all bays was measured in spring 2017 ($\bar{x}$: 724.6±72.5 dpm·m^{-3}) followed by summer 2017 ($\bar{x}$: 640.8±64.1 dpm·m^{-3}).

Activities of ^{224}Ra were in average 1400.5±140.1 dpm·m^{-3} across all seasons for all the bays. As with ^{226}Ra, the highest average ^{224}Ra surface water activity was measured in spring 2017 ($\bar{x}$: 2350.4±235.0 dpm·m^{-3}) in Baffin Bay and the lowest also occurred in winter 2018 ($\bar{x}$: 492.1±49.2 dpm·m^{-3}), in Laguna Madre (**Figure 7B; Table 7**)**.** The highest average activities of all four seasons were found in Aransas Bay ($\bar{x}$: 1835.9±183.6 dpm·m^{-3}) while the lowest in Laguna Madre ($\bar{x}$: 846.6±84.7 dpm·m^{-3}). Across the four seasons, the lowest activities were almost consistently measured in Laguna Madre followed by Oso Bay. Across all bays, similar to ^{226}Ra, the lowest average ^{224}Ra ($\bar{x}$: 914.9±91.5 dpm·m^{-3}) was measured in winter 2018 followed by winter 2017 ($\bar{x}$: 1359.3±13.6 dpm·m^{-3}). Also, the highest average activity across all bays was

measured in spring 2017 ($\bar{x}$: 1828.5±182.9 dpm·m^{-3}) followed by summer 2017 ($\bar{x}$: 1431.9±143.2 dpm·m^{-3}).

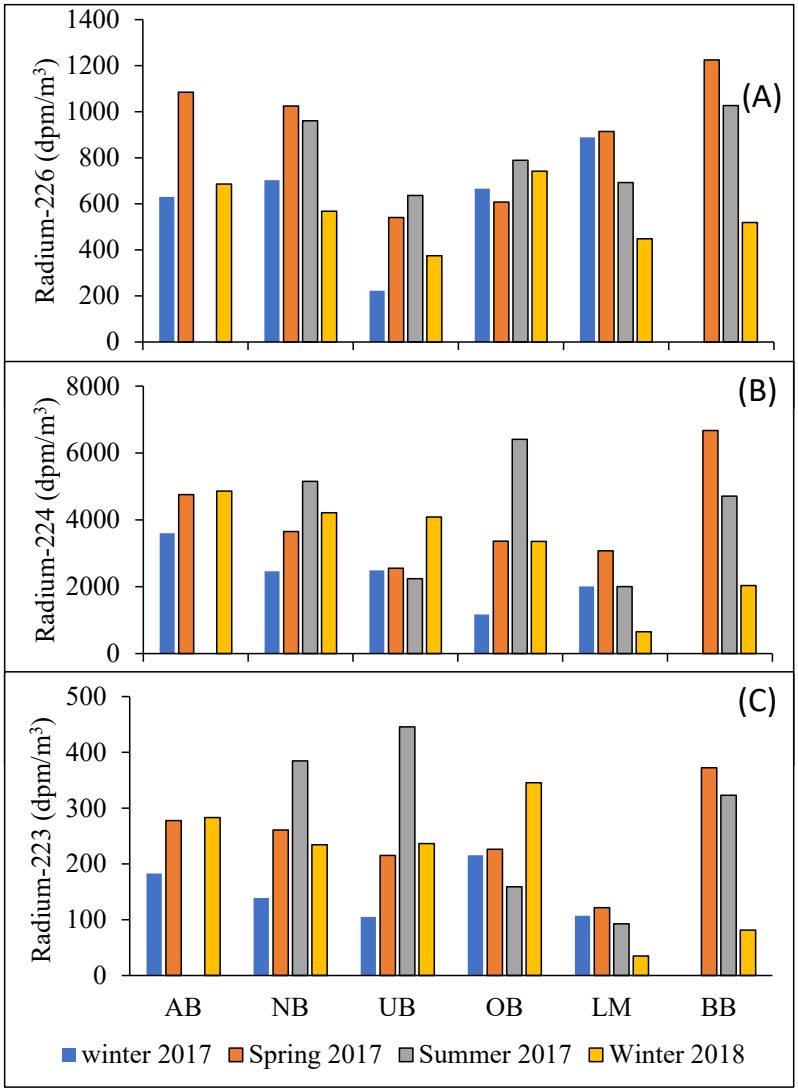

Figure 7. Average (A) Radium-226, (B) Radium-224, and (C) Radium-223 activities (dpm/m^3) across the six sampling sites and seasons. Sampling sites are denoted as: AB-Aransas Bay, NB-Nueces Bay, UB-University Beach, OB-Oso Bay, LM-Laguna Madre, and BB-Baffin Bay.

Activities of ^{223}Ra follow a similar pattern as ^{224}Ra, showing more enrichment in the northern bays and lower activities in the southernmost areas such as Laguna Madre and Baffin Bay. ^{223}Ra were in average 115.4±11.5 dpm·m^{-3} across all seasons for all the bays. The highest average ^{223}Ra surface water activity was measured in spring 2017 ($\bar{x}$: 219.0±21.9 dpm·m^{-3}) at the

University Beach and Nueces Bay ($\overline{x}$: 201.2±20.1 dpm·m^{-3}). The lowest average activities occurred in winter 2018 in Baffin Bay and Laguna Madre ($\overline{x}$: 39.9±4.0 and 39.7±4.0 dpm·m^{-3}, respectively) and winter 2017 in Laguna Madre and Baffin Bay ($\overline{x}$: 48.8±4.9 and 55.9±5.6 dpm·m^{-3}, respectively) (**Figure 7C; Table 7**)**.** The highest average activities of all four seasons were found in Nueces Bay ($\overline{x}$: 143.9±14.4 dpm·m^{-3}), although University Beach, Oso Bay and Aransas Bay follow closely ($\overline{x}$: 143.2±14.3, 128.2±12.8 and 126.1±12.6 dpm·m^{-3}, respectively). The lowest overall average ^{223}Ra occurred in Laguna Madre ($\overline{x}$: 60.1±6.0 dpm·m^{-3}) followed by Baffin Bay ($\overline{x}$: 90.9±9.1 dpm·m^{-3}). Across the four seasons, the lowest activities were consistently measured in Laguna Madre. Across all bays, similar to other two isotopes, the lowest average ^{223}Ra ($\overline{x}$: 68.6±6.9 dpm·m^{-3}) was measured in winter 2018 followed by winter 2017 ($\overline{x}$: 102.4±10.2 dpm·m^{-3}). Also, the highest average activity across all bays was measured in spring 2017 ($\overline{x}$: 163.8±16.4 dpm·m^{-3}) followed by summer 2017 ($\overline{x}$: 127.0±12.7 dpm·m^{-3}).

Table 7. Surface water radium (dpm·m^{-3}) and radon (Bq·m^{-3}) activities for each of the bays of interest presented as the minimum, maximum, and average value for each sampling event. † Winter 2017 NB samples were collected from station 7 from Murgulet et al. (2018). ‡ Winter 2017 BB samples are from station 11 from Lopez et al. (2018).

		AB			NB†			UB			OB			LM			BB‡		
		Min.	Max.	Avg.	Min.	Max.	Avg.	Min.	Max.	Avg.	Min.	Max.	Avg.	Min.	Max.	Avg.	Min.	Max.	Avg.
December 2016 - January 2017	^{223}Ra	150.4	203.1	176.8	83.7	99.7	90.7	81.5	128.5	105.0	124.5	150.0	137.3	42.2	55.3	48.8	53.0	58.7	55.9
	^{224}Ra	2,983.0	3,268.0	3,125.5	834.1	1,084.7	921.7	865.6	1,474.9	1,170.3	1,303.1	1,484.6	1,393.8	728.9	818.1	773.5	739.5	803.3	771.4
	^{226}Ra	495.7	580.5	538.1	254.1	502.4	378.3	53.0	392.0	222.5	483.9	483.9	483.9	354.5	360.6	357.6	867.4	867.4	867.4
	^{222}Rn	69.9	223.0	138.3	108.0	171.0	136.8	20.8	116.0	64.1	57.7	158.0	94.4	9.3	29.0	22.5	11.3	58.1	46.2
April - June 2017	^{223}Ra	77.1	158.2	116.7	169.6	242.8	201.2	218.9	219.1	219.0	157.2	165.5	161.4	72.4	97.8	87.8	127.5	298.7	196.6
	^{224}Ra	1,217.4	1,776.5	1,411.8	1,706.5	2,672.0	2,064.4	1,693.1	2,559.8	2,126.5	1,633.3	2,072.2	1,852.7	1,097.4	1,237.8	1,165.1	1,377.7	4,039.2	2,350.4
	^{226}Ra	422.5	584.4	514.7	604.5	866.1	785.0	398.6	398.6	398.6	373.1	373.1	373.1	652.7	652.7	652.7	1,204.7	1,842.7	1,623.7
	^{222}Rn	20.6	160.0	68.2	135.0	252.0	194.4	195.0	418.0	325.6	84.4	377.0	179.5	19.1	30.7	26.1	27.1	48.0	39.1
August - September 2017	^{223}Ra	Goose Island State Park closed due to Hurricane Harvey damage.			189.6	239.8	206.7	178.5	190.9	182.8	98.9	121.5	110.2	63.7	64.5	64.1	51.5	100.8	71.3
	^{224}Ra				1,754.7	2,087.6	1,929.6	1,558.7	1,876.3	1,706.2	1,544.8	1,614.7	1,579.7	952.1	959.4	955.7	782.5	1,235.3	988.4
	^{226}Ra				550.4	829.1	730.4	410.7	578.1	494.4	502.2	604.2	553.2	435.9	446.3	441.1	984.9	984.9	984.9
	^{222}Rn				137.0	254.0	200.2	35.3	339.0	164.5	88.8	561.0	264.4	39.6	67.3	53.8	15.7	27.9	23.2
December 2017 - January2018	^{223}Ra	75.7	93.8	84.8	67.0	85.3	77.1	59.4	78.8	66.2	36.0	179.9	104.1	36.4	43.1	39.7	37.0	44.0	39.9
	^{224}Ra	950.7	990.1	970.4	875.9	1,140.8	993.0	682.5	950.5	832.1	547.2	2,808.6	1,559.2	486.0	498.2	492.1	540.4	704.1	642.6
	^{226}Ra	497.4	497.6	497.5	381.6	435.3	411.5	270.2	316.2	286.9	228.1	685.5	424.4	29.0	343.0	186.0	653.3	653.3	653.3
	^{222}Rn	61.5	132.0	105.0	1.9	299.0	184.6	60.0	755.0	503.6	60.0	371.0	233.8	14.9	22.4	18.1	7.0	22.7	14.3
Overall Avg.	^{223}Ra	101.1	151.7	126.1	127.5	166.9	143.9	134.6	154.3	143.2	104.1	154.2	128.2	53.7	65.2	60.1	67.3	125.6	90.9
	^{224}Ra	1,717.0	2,011.5	1,835.9	1,292.8	1,746.3	1,477.2	1,200.0	1,715.4	1,458.7	1,257.1	1,995.0	1,596.4	816.1	878.4	846.6	860.0	1,695.4	1,188.2
	^{226}Ra	471.9	554.2	516.8	447.6	658.2	576.3	283.1	421.2	350.6	396.8	536.7	458.7	368.0	450.7	409.3	927.6	1,087.1	1,032.3
	^{222}Rn	50.7	171.7	103.8	95.5	244.0	179.0	77.8	407.0	264.5	72.7	366.8	193.0	20.7	37.4	30.1	15.3	39.2	30.7

Porewater Radium Activities

Activities of ^{226}Ra were in average 841.0±84.1 dpm·m^{-3} across all seasons for all the bays. The highest average ^{226}Ra porewater activity was measured in winter 2017 ($\bar{x}$: 1419.7±141.2 dpm·m^{-3}) in Laguna Madre, while the lowest occurred in winter 2018 in Aransas Bay and University Beach ($\bar{x}$: 343.6±34.4 and 415.0±41.5 dpm·m^{-3}, respectively) (**Figure 7A**; **Table 7).** The highest average activities of all four seasons were found in Nueces Bay ($\bar{x}$: 1127.9±112.8 dpm·m^{-3}). Laguna Madre also showed overall enrichment over the other locations with an average seasonal ^{226}Ra of 1003.6±10.0 dpm·m^{-3}. As with surface water, the lowest at seasonal average ^{226}R activity was measured in porewater at the University Beach ($\bar{x}$: 526.5±52.7 dpm·m^{-3}). The lowest activities were consistently measured at the University Brach followed by Baffin Bay. Like surface water, across all bays, the lowest average ^{226}Ra ($\bar{x}$: 547.8±54.8 dpm·m^{-3}) was measured in winter 2018. However, as opposed to surface water, winter 2017 exhibits the largest all bays average ($\bar{x}$: 1122.6±112.3 dpm·m^{-3}). The next highest average activity across all bays was measured in spring 2017 ($\bar{x}$: 1012.2±101.2 dpm·m^{-3}) when the highest surface water activity was measured. This is followed by summer 2017 ($\bar{x}$: 928.2±92.8 dpm·m^{-3}).

Activities of ^{224}Ra are present in high activities in porewater. In average ^{224}Ra activity, across all seasons for all the bays, was 5616.4±561.4 dpm·m^{-3}, which is almost five orders of magnitude higher than surface water ($\bar{x}$: 1400.5±140.1 dpm·m^{-3}). As in surface water, the highest average ^{224}Ra porewater activities were measured in summer 2017 at the University Beach ($\bar{x}$: 11113.6±1111.4 dpm·m^{-3}) and Nueces Bay ($\bar{x}$: 8374.2±837.4 dpm·m^{-3}) and in spring 2017 in Baffin bay ($\bar{x}$: 10999.2±1100 dpm·m^{-3}). The lowest average activities occurred in winter 2018 in Laguna Madre ($\bar{x}$: 1598.0±159.8 dpm·m^{-3}) and winter 2017 in Baffin Bay ($\bar{x}$: 2250.5±9.1 dpm·m^{-3}) (**Table 8).**

The highest average activities of all four seasons were found at University Beach ($\bar{x}$: 8213.7±821.4 dpm·m^{-3}), followed by Nueces Bay ($\bar{x}$: 6627.3±662.7 dpm·m^{-3}). Like ^{223}Ra, the two locations follow the same trend for the spring and summer 2017 and winter 2018; but, because data for Nueces Bay are not available for winter 2017, the average could be more biased towards this bay. The lowest seasonal average ^{224}Ra occurred in Laguna Madre ($\bar{x}$: 3218.4±321.8 dpm·m^{-3}), also the location with the lowest activity in surface water ($\bar{x}$: 846.6±84.7 dpm·m^{-3}). Oso Bay also shows one of the most depleted activities in porewater ($\bar{x}$: 3813.2±381.3 dpm·m^{-3}) when compared to all other bays, which are similar in their seasonal average. As with surface water and ^{223}Ra, across the four seasons, the lowest activities were consistently measured in Laguna Madre. Across all bays, the lowest average ^{224}Ra was measured in winter 2017 ($\bar{x}$: 3711.1±371.1 dpm·m^{-3}) followed by winter 2018 ($\bar{x}$: 5176.5±517.7 dpm·m^{-3}). The highest average activity across all bays was measured in summer 2017 ($\bar{x}$: 7690.7±769.1 dpm·m^{-3}) followed by spring 2017 ($\bar{x}$: 6131.4±613.1 dpm·m^{-3}).

Activities of ^{223}Ra show overall more enrichment in the Nueces bay and University Beach. ^{223}Ra activities were in average (average across all seasons for all the bays: 316.9±31.7 dpm·m^{-3}) about three times larger than surface water activities. As in surface water, the highest average ^{223}Ra porewater activities were measured in summer 2017 at the University Beach ($\bar{x}$: 708.6±70.9 dpm·m^{-3}) and Nueces Bay ($\bar{x}$: 562.5±56.2 dpm·m^{-3}). The lowest average activities occurred in winter 2018 in Laguna Madre ($\bar{x}$: 69.8±7.0 dpm·m^{-3}) and winter 2017 in Baffin Bay ($\bar{x}$: 90.5±9.1 dpm·m^{-3}) (**Figure 7C; Table 7**).

Table 8. Porewater radium (dpm·m^{-3}) and radon (Bq·m^{-3}) activities for each of the bays of interest presented as the maximum, minimum, and average value for each sampling event. † Winter 2017 NB samples were collected from station 7 from Murgulet et al. (2018). ‡ Winter 2017 BB samples are from station 11 from Lopez et al. (2018).

		AB			NB†			UB			OB			LM			BB‡		
		Min.	Max.	Avg.	Min.	Max.	Avg.	Min.	Max.	Avg.	Min.	Max.	Avg.	Min.	Max.	Avg.	Min.	Max.	Avg.
December 2016 - January 2017	^{223}Ra	195.1	195.1	195.1	244.7	244.7	244.7	--	--	--	199.6	300.7	254.8	70.4	260.3	165.4	58.4	122.7	90.5
	^{224}Ra	4,554.0	4,554.0	4,554.0	5,465.3	5,465.3	5,465.3	--	--	--	2,990.5	3,084.9	3,039.1	1,964.2	4,528.7	3,246.4	1,937.7	2,563.3	2,250.5
	^{226}Ra	814.4	1,094.0	954.2	1,211.6	1,351.4	1,281.5	--	--	--	730.5	939.4	834.9	1,227.3	1,612.0	1,419.7	--	--	--
	^{222}Rn	--	--	--	274.3	1,277.6	776.0	--	--	--	3,095.0	7,114.6	5,030.2	64.4	154.6	109.5	34.6	34.6	34.6
April - June 2017	^{223}Ra	209.0	252.8	238.5	152.2	567.2	320.6	376.8	394.1	385.5	356.0	356.0	356.0	107.0	187.0	147.0	416.9	669.3	548.2
	^{224}Ra	4,304.6	5,364.8	4,901.7	3,356.9	8,963.6	5,236.3	6,063.4	7,374.1	6,718.8	3,956.6	3,956.6	3,956.6	4,842.5	5,109.2	4,975.8	9,382.5	12,669.0	10,999.2
	^{226}Ra	960.1	1,519.4	1,194.6	957.6	1,719.1	1,264.2	453.7	592.8	523.3	950.2	950.2	950.2	955.2	1,302.8	1,129.0	--	--	--
	^{222}Rn	162.8	371.3	256.6	2,858.2	4,617.8	3,738.0	1,291.2	1,589.3	1,440.3	4,167.6	4,167.6	4,167.6	214.9	403.7	309.3	44.2	386.2	196.4
August - September 2017	^{223}Ra	Goose Island State Park closed due to Hurricane Harvey damage.			490.1	624.9	562.5	638.1	819.9	708.6	--	--	--	93.3	149.3	121.3	393.8	618.0	493.8
	^{224}Ra				7,895.7	9,203.3	8,374.2	10,783.3	11,584.3	11,113.6	--	--	--	2,834.9	3,271.6	3,053.2	7,078.5	9,723.2	8,221.9
	^{226}Ra				747.9	1,373.1	1,079.8	641.3	641.3	641.3	--	--	--	884.1	1,004.2	944.1	964.9	1,130.5	1,047.7
	^{222}Rn				1,927.5	3,854.7	2,721.1	--	--	--	--	--	--	124.7	173.6	149.2	--	--	--
December 2017 - January2018	^{223}Ra	260.3	403.5	331.9	351.8	419.6	391.8	422.4	583.3	495.0	233.5	327.1	280.3	30.0	117.4	69.8	112.9	137.4	122.9
	^{224}Ra	6,933.6	7,759.9	7,346.7	6,155.5	8,282.9	7,433.3	5,812.3	7,346.7	6,808.9	3,244.0	5,643.7	4,443.9	720.0	2,515.4	1,598.0	3,208.8	3,820.1	3,428.5
	^{226}Ra	343.6	343.6	343.6	738.6	1,101.5	885.9	374.7	483.0	415.0	730.9	730.9	730.9	508.8	534.6	521.7	340.7	438.9	389.8
	^{222}Rn	-	213.2	106.6	1,532.1	2,845.0	2,296.6	--	--	--	--	--	--	126.0	174.0	150.0	--	--	--
Overall Average	^{223}Ra	221.5	283.8	255.2	309.7	464.1	379.9	479.1	599.1	529.7	263.0	327.9	297.0	75.2	178.5	125.9	245.5	386.8	313.9
	^{224}Ra	5,264.1	5,892.9	5,600.8	5,718.3	7,978.8	6,627.3	7,553.0	8,768.4	8,213.7	3,397.1	4,228.4	3,813.2	2,590.4	3,856.2	3,218.4	5,401.9	7,193.9	6,225.0
	^{226}Ra	706.1	985.7	830.8	913.9	1,386.3	1,127.9	489.9	572.4	526.5	803.9	873.5	838.7	893.8	1,113.4	1,003.6	652.8	784.7	718.8
	^{222}Rn	81.4	292.2	181.6	1,648.0	3,148.8	2,382.9	1,291.2	1,589.3	1,440.3	3,631.3	5,641.1	4,598.9	132.5	226.5	179.5	39.4	210.4	115.5

The highest average activities of all four seasons were found at University Beach ($\bar{x}$: 529.7±53.0 dpm·m^{-3}), although Nueces Bay follows very closely ($\bar{x}$: 376.9±37.7 dpm·m^{-3}). The two locations follow the same trend for the spring and summer 2017 and winter 2018; but, because data for Nueces Bay are not available for winter 2017, the average could be more biased towards this bay. The lowest seasonal average ^{223}Ra occurred in Laguna Madre ($\bar{x}$: 125.9±12.6 dpm·m^{-3}), also the location with the lowest activity in surface water ($\bar{x}$: 60.1±6.0 dpm·m^{-3}). The rest of the bays are similar in their seasonal average. As with surface water, across the four seasons, the lowest activities were consistently measured in Laguna Madre. Across all bays, the lowest average ^{223}Ra was measured in winter 2017 ($\bar{x}$: 190.1±19.0 dpm·m^{-3}) followed by winter 2018 ($\bar{x}$: 281.9±28.2 dpm·m^{-3}). The highest average activity across all bays was measured in summer 2017 ($\bar{x}$: 471.5±47.2 dpm·m^{-3}) followed by spring 2017 ($\bar{x}$: 332.6±33.3 dpm·m^{-3}).

Submarine Groundwater Discharge

^{222}Rn-derived SGD estimates

Previous studies have shown that selection of a representative groundwater endmember for estimation of SGD fluxes is challenging (Burnett and Dulaiova 2003; Cerdà-Domènech et al. 2017; Garcia-Orellana et al. 2013; Lamontagne et al. 2008; Urquidi-Gaume et al. 2016) as it can result in a large range of magnitudes. Deep groundwater input is expected to be limited given the potential isolation of deeper aquifers from the bay bottoms with confining units. Nevertheless, deeper groundwater input may be expected in Nueces Bay (Murgulet et al. 2018). Given that other studies in the south Texas coastal area found similar ranges in ^{222}Rn activities in the shallow/unconfined and deeper semiconfined aquifers, the deep groundwater activities are also considered in the SGD estimates. To account for these possible uncertainties related to the groundwater endmember, for SGD estimates the following groundwater endmembers were used:

(1) the highest porewater measured at each location for the duration of the study; (2) the average of all wells within the south Texas coastal area (i.e. avg. regional) and (3) the average groundwater radon activities within each watershed (avg. watershed) (**Table 9**). SGD rates calculated with the regional average of groundwater is used for reporting and nutrient flux calculations. The average porewater and lowest groundwater ^{222}Rn activities yield SGD rates that are relatively high when considering the subsurface characteristics (e.g., lithologic characteristics) and hydrologic conditions as well as the climate in the area. These estimates are deemed as the least conservative and most unrealistic and are not included in this study's discussion.

Table 9. Radon endmembers for radon-derived SGD calculations

Bay	Highest PW	Avg. Regional	Avg. Watershed
AB	10,837	10,613	16,039
NB	13,790	10,613	7,016
UB	7,115	10,613	6,601
OB	7,115	10,613	6,601
LM	865	10,613	7,282
BB	1,557	10,613	7,805

Overall, the largest SGD rates occur in Nueces Bay and at the University Beach (seasons average: 109 and 107 cm/d, respectively) while the lowest occurred in Baffin Bay, Laguna Madre and Aransas Bay (seasons average: 15, 19 and 28 cm/d, respectively) (**Figure 8; Table 10**). Oso Bay rates are very similar across seasons ranging from 56 cm/d (spring 2017) to 73 cm/d in winter 2017. The highest SGD rate among all bays was measured in winter 2018 at University Beach (233 cm/d). In winter 2018, a higher SGD, when compared to other seasons, was also measured in Aransas Bay (44.7 cm/d), but the rate is smaller than any of the ones measured in Nueces Bay and University Beach and approaching the one in Oso Bay (50.8 cm/d).

Based on a 24-hour survey, or less, conducted approximately every 3 months, there is no evidence of a seasonal fluctuation that applies across all bays. This could result from the choice of a fixed endmember, rather than one for each season, which could overestimate or underestimate SGD rates and mask a seasonal trend across the systems. Nevertheless, each of these systems are likely to be influenced by different human and hydroclimatic stressors, as well as are underlined by different lithologies, thus, the seasonal response may be variable.

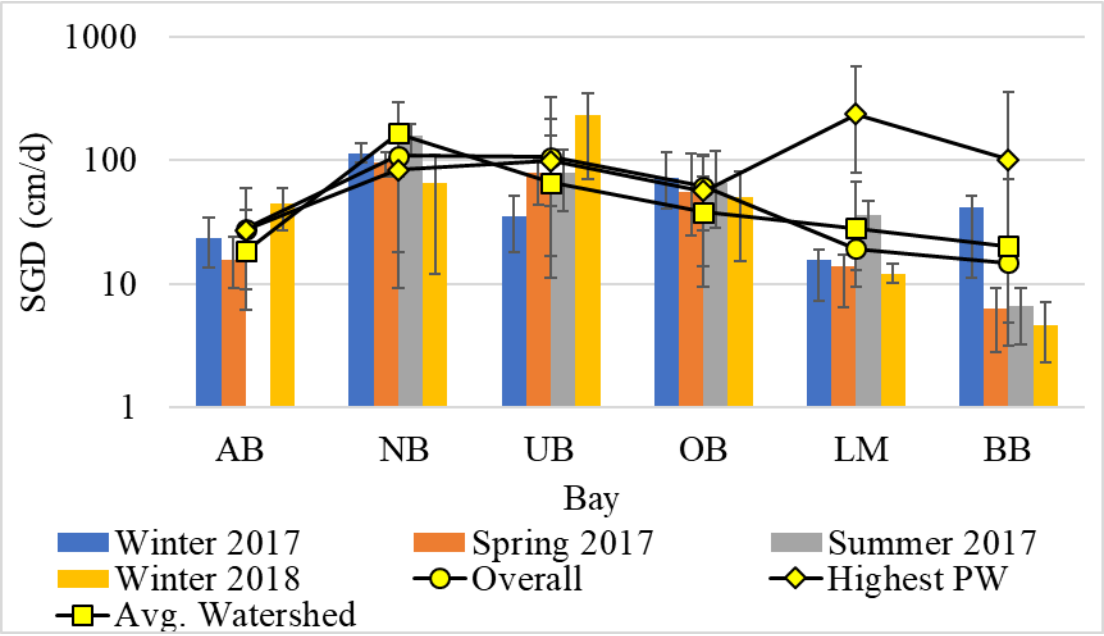

Figure 8. Seasonal and spatial variation of SGD (cm/d). Error bars represent the minimum and maximum SGD rate observed during the time series measurements. Bay averages are included for the three different endmembers used to convert radon inventories into SGD rates.

Table 10. SGD rates (in cm/d) calculated from time series ^{222}Rn measurements. Included are the minimum, maximum, average, and standard deviation of the SGD rates calculated for each sampling event using three possible Rn activity endmembers (see also **Table 9**): the highest measured Rn activity in bay porewater, the average groundwater Rn activity measured in the bay's watershed, and the average Rn activity of 33 regional wells.

		December 2016 - January 2017			April - June 2017			August - October 2017			December 2017 - January 2018			
		Highest PW	Avg. Watershed	Avg. Regional	Highest PW	Avg. Watershed	Avg. Regional	Highest PW	Avg. Watershed	Avg. Regional	Highest PW	Avg. Watershed	Avg. Regional	Overall Avg.
AB	Min.	13.4	9.1	13.7	9.1	6.1	9.3	Goose Island State Park closed due to Hurricane Harvey damage.			26.3	17.7	26.8	16.6
	Max.	33.9	22.9	34.6	23.6	15.9	24.1				59.1	39.9	60.4	39.7
	Avg.	23.1	15.6	**23.6**	15.2	10.3	**15.6**				43.7	29.6	**44.7**	**27.9**
	Stdev	3.9	2.7	4.0	4.4	3.0	4.5				8.0	5.4	8.2	5.5
NB†	Min.	74.6	146.7	97.0	57.3	112.5	74.4	85.0	167.1	110.4	9.3	18.2	12.0	73.5
	Max.	105.0	206.3	136.4	90.5	177.9	117.6	151.1	296.9	196.3	86.4	169.8	112.3	140.6
	Avg.	88.5	174.0	**115.0**	73.7	144.8	**95.7**	122.0	239.7	**158.5**	51.1	100.5	**66.4**	**108.9**
	Stdev	9.1	17.9	11.8	7.5	14.7	9.7	18.6	36.5	24.2	23.8	46.7	30.9	19.1
UB	Min.	16.9	11.3	18.2	40.2	26.9	43.3	36.1	24.2	38.9	65.7	44.0	70.8	42.8
	Max.	48.3	32.4	52.1	96.7	64.8	104.2	114.6	76.9	123.6	323.7	217.0	348.9	157.2
	Avg.	32.5	21.8	**35.1**	74.3	49.8	**80.0**	72.9	48.9	**78.6**	215.8	144.7	**232.6**	**106.6**
	Stdev	7.7	5.2	8.3	17.8	11.9	19.2	25.5	17.1	27.5	79.5	53.3	85.7	35.2
OB	Min.	38.1	25.6	41.1	22.7	15.2	24.5	26.3	17.6	28.4	14.0	9.4	15.1	27.3
	Max.	107.8	72.3	116.2	106.5	71.4	114.8	111.3	74.6	120.0	76.0	51.0	81.9	108.2
	Avg.	67.7	45.4	**72.9**	51.5	34.6	**55.6**	60.8	40.8	**65.6**	47.1	31.6	**50.8**	**61.2**
	Stdev	17.4	11.7	18.8	28.4	19.1	30.7	20.8	13.9	22.4	19.4	13.0	20.9	23.2
LM	Min.	89.8	10.7	7.3	80.3	9.5	6.5	336.2	39.9	27.4	125.9	15.0	10.3	12.9
	Max.	230.7	27.4	18.8	210.6	25.0	17.2	571.5	67.9	46.6	180.6	21.5	14.7	24.3
	Avg.	190.7	22.7	**15.5**	172.5	20.5	**14.1**	440.5	52.3	**35.9**	148.6	17.6	**12.1**	**19.4**
	Stdev	45.5	5.4	3.7	37.1	4.4	3.0	69.2	8.2	5.6	20.1	2.4	1.6	3.5
BB‡	Min.	75.9	15.2	11.1	19.1	3.8	2.8	22.1	4.4	3.2	15.7	3.1	2.3	4.9
	Max.	354.2	70.7	52.0	62.7	12.5	9.2	63.2	12.6	9.3	48.1	9.6	7.1	19.4
	Avg.	286.0	57.0	**42.0**	42.8	8.5	**6.3**	45.1	9.0	**6.6**	31.3	6.2	**4.6**	**14.9**
	Stdev	78.1	15.6	11.5	9.9	2.0	1.5	11.5	2.3	1.7	8.9	1.8	1.3	4.0

The SGD rates reported here align with measurements from previous work in Aransas, Nueces, Corpus and Baffin Bays. For instance, in Nueces Bay large SGD rates have been measured during a two-year seasonal study and significant variability was observed spatially and seasonally (Murgulet et al. 2018). In addition, in Corpus Christi Bay, besides the large SGD rates measured in 2015, the highest magnitude was measured in late summer-fall (Murgulet et al. 2015), similar to this study (**Figure 8**). Aransas and Baffin bays were among the bays with the lowest SGD (Lopez et al. 2018; Spalt et al. 2018).

Long-term ^{222}Rn-derived SGD estimates at the University Beach

SGD rates derived from the long-term continuous measurements of radon at the University Beach platform show some significant monthly and seasonal variabilities when compared to the 2017 four season, 24-hour monitoring events (**Figure 9; Table 10; Table 11**). Both types of measurements indicate that winter 2018 exhibits the highest SGD rates (up to 200 cm/d). Both records indicate that SGD is decreasing during the hot and dry summer months.

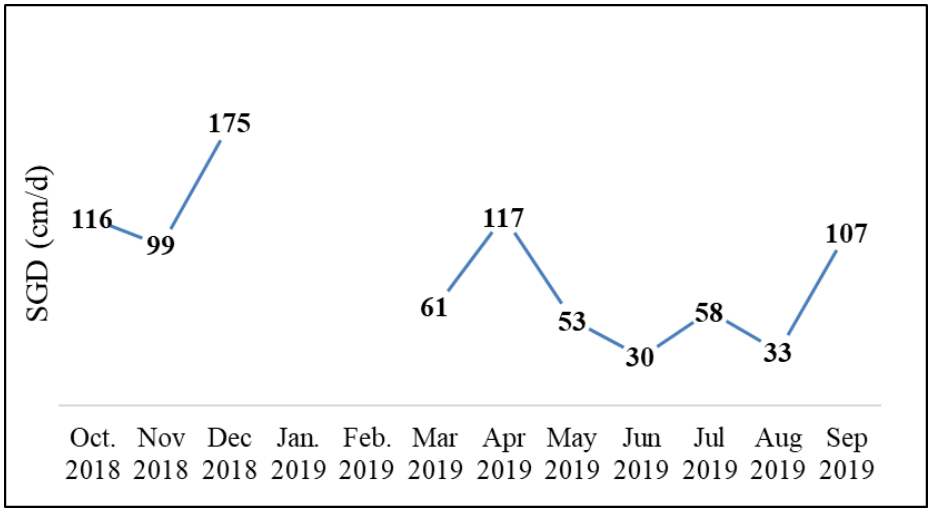

Figure 9. Average monthly SGD (cm/d) at the University Beach as part of the continuous monitoring effort. The rates presented here are those calculated using the average regional groundwater radon endmember. See **Table 11** for the Min, Max, Avg. and St. Dev of SGD as well as the different radon endmember-derived SGD rates.

Table 11. Monthly average SGD rates (in cm/d) calculated from time series ^{222}Rn measurements at the University Beach platform. Included are the minimum, maximum, average, and standard deviation of the SGD rates calculated for each sampling event using three Rn activity endmembers (see also **Table 9**).

		Highest PW	Avg. Watershed	Avg. Regional			Highest PW	Avg. Watershed	Avg. Regional
Oct. 2018	Min.	55.6	37.3	59.9	May 2019	Min.	28.4	19.0	30.6
	Max.	178.5	119.6	192.3		Max.	90.3	60.5	97.3
	Avg.	107.8	72.3	116.2		Avg.	48.7	32.7	52.5
	Stdev	23.0	15.4	24.8		Stdev	9.6	6.4	10.3
	n	206	206	206		n	127	127	127
Nov 2018	Min.	46.4	31.1	50.1	Jun 2019	Min.	12.2	8.2	13.2
	Max.	166.6	111.7	179.6		Max.	52.5	35.2	56.6
	Avg.	91.9	61.6	99.0		Avg.	27.7	18.5	29.8
	Stdev	32.6	21.9	35.2		Stdev	9.5	6.3	10.2
	n	359	359	359		n	109	109	109
Dec 2018	Min.	48.2	32.3	52.0	Jul 2019	Min.	27.0	18.1	29.1
	Max.	267.1	179.1	287.9		Max.	203.0	136.1	218.8
	Avg.	162.7	109.1	175.4		Avg.	54.0	36.2	58.2
	Stdev	49.2	32.9	53.0		Stdev	19.7	13.2	21.2
	n	135	135	135		n	875	875	875
Mar 2019	Min.	17.5	11.7	18.9	Aug 2019	Min.	6.5	7.1	11.5
	Max.	110.6	74.1	119.2		Max.	136.9	91.8	147.5
	Avg.	53.3	38.2	61.4		Avg.	27.3	21.6	33.2
	Stdev	18.7	13.9	22.3		Stdev	24.9	16.1	25.6
	n	335	335	335		n	424	424	424
Apr 2019	Min.	57.3	38.4	61.8	Sep 2019	Min.	25.5	17.1	27.5
	Max.	235.9	158.1	254.2		Max.	267.2	179.1	287.9
	Avg.	108.5	72.8	117.0		Avg.	99.0	66.3	106.6
	Stdev	31.3	21.0	33.8		Stdev	45.8	30.7	49.4
	n	121	121	121		n	1147	1147	1147

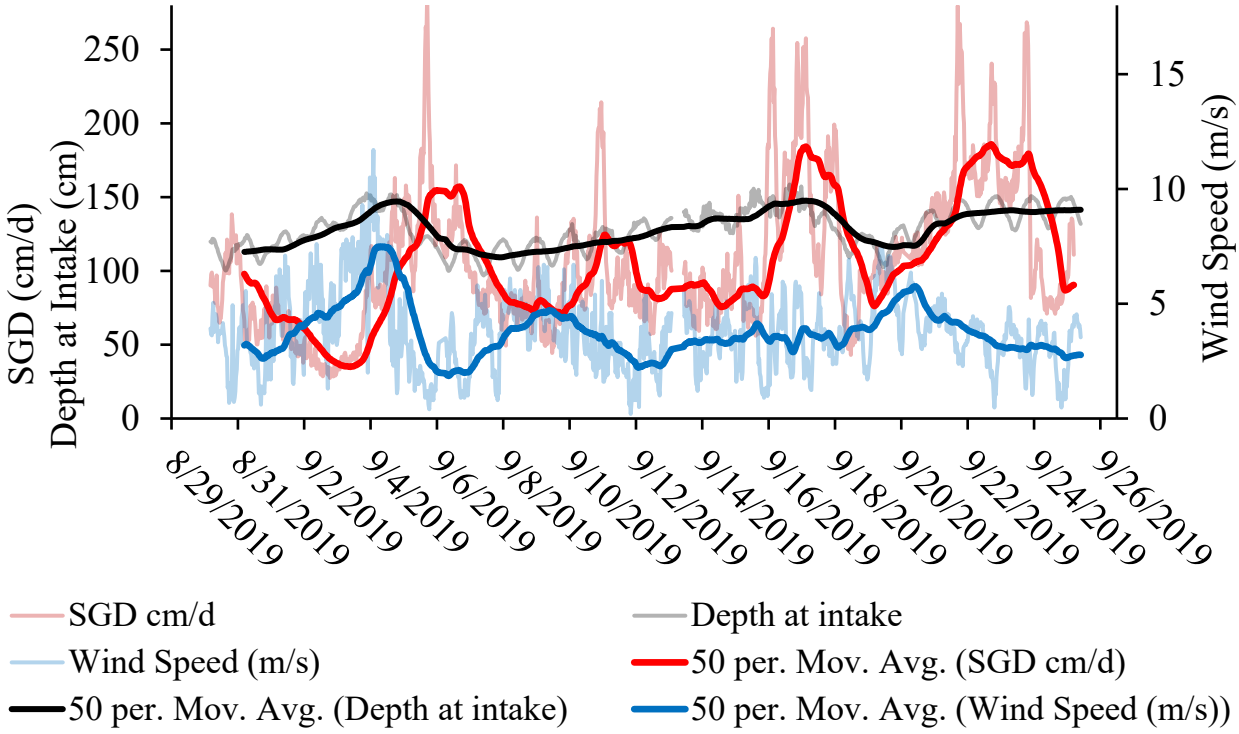

Figure 10. Continuous/hourly SGD measurements at the University Beach platform September 2019.

The hourly SGD measurements presented in **Figure 10** (above) show significant fluctuations in rates which are not related to tidal changes. Most studies indicate that SGD increases at low tide and decreases at high tide. However, at University Beach, higher tides tend to be followed by significant increases in SGD rates. Wind speed and SGD rates show an inverse relationship; thus, degassing may be responsible for the decrease in SGD rates. Degassing was shown to alter SGD rates in Copano Bay (Spalt et al. 2018) and Oso Bay (Lopez et al. 2018).

^{226}Ra-derived SGD estimates

The ^{224}Ra/^{223}Ra activity ratio (AR) measured in the porewaters each season was compared to those of surface water to derive radium water ages (Knee et al. 2011). These ARs

were used to calculate water ages that were plugged into the radium inventory which were converted to advective fluxes (**Table 12**) using the ^{223}Ra and ^{226}Ra of the porewater.

Table 12. Radium based SGD rates calculated for the bays using porewater radium activities as the endmember. SGD values are presented in cm/d. Uncertainty for SGD is derived from the uncertainty of the radium measurements which is on average 10%. † Winter 2017 NB samples were collected from station 7 from Murgulet et al. (2018). ‡ Winter 2017 BB samples are from station 11 from Lopez et al. (2018). Average radon-derived SGD rates (in cm/d) determined using the three different groundwater/porewater radon endmembers are also included for reference with uncertainties that represent the 2 standard deviations of all event time series measurements.

		AB	NB†	UB	OB	LM	BB‡
December 2016 - January 2017	^{223}Ra	--	4±0.4	2±0.2	26±2.6	9±0.9	29±2.9
	^{226}Ra	3±0.3	3±0.3	--	16±1.6	15±1.5	7±0.7
	^{222}Rn (high)	34±4	174±18	35±8	73±19	191±46	286±78
	^{222}Rn (mid)	16±2.7	115±12	22±5	68±17	23±5	57±16
	^{222}Rn (low)	9±3.9	89±9	33±8	45±12	16±4	42±12
April - June 2017	^{223}Ra	--	11±1.1	6±0.6	3±0.3	3±0.3	26±2.6
	^{226}Ra	23±2.3	10±1.0	5±0.5	18±1.8	4±0.4	21±2.1
	^{222}Rn (high)	16±5	145±15	80±19	56±31	173±37	43±10
	^{222}Rn (mid)	15±4	96±10	74±18	52±28	21±4	9±2
	^{222}Rn (low)	10±3	74±8	50±12	35±19	14±3	6±2
August - September 2017	^{223}Ra	Goose Island State Park closed due to Hurricane Harvey damage	12±1.2	10±1.0	--	4±0.4	100±10.0
	^{226}Ra		11±1.1	7±0.7	--	8±0.8	59±5.9
	^{222}Rn (high)		240±37	79±28	66±22	441±69	45±12
	^{222}Rn (mid)		159±24	73±26	61±21	52±8	9±2
	^{222}Rn (low)		122±19	49±17	41±14	36±6	7±2
December 2017 - January2018	^{223}Ra	--	12±1.2	41±4.1	105±10.5	--	22±2.2
	^{226}Ra	8±0.8	6±0.6	1±0.1	126±12.6	2±0.2	10±0.1
	^{222}Rn (high)	45±8	101±47	233±86	51±21	149±4	31±9
	^{222}Rn (mid)	44±8	66±31	216±80	47±19	18±2	6±2
	^{222}Rn (low)	30±5	51±24	145±53	32±13	12±2	5±1

Using the seasonal porewater ^{226}Ra endmembers and corresponding surface water radium ages, SGD rates ranged between 1±0.1 cm/d at the University Beach in winter 2018 and 126±12.6 cm/d at Oso Bay, also in winter 2018. Using the seasonal porewater ^{223}Ra endmembers, SGD rates ranged between 2±0.2 cm/d at the University Beach in winter 2017 and 105±10.5 cm/d at Oso Bay. The highest radium-derived SGD rates occur in Oso Bay (bay

seasons average of ^{226}Ra and ^{223}Ra: 53±5.3 and 45±4.5 cm/d, respectively). The lowest seasonal average occurred in Laguna Madre (bay seasons average of ^{226}Ra and ^{223}Ra: 5±0.5 and 7±0.7 cm/d, respectively) and Nueces Bay (bay seasons average of ^{226}Ra and ^{223}Ra: 10±1.0 and 8±0.8 cm/d, respectively). Seasonally, the lowest SGD rates occurred in winter (all bay average of ^{226}Ra and ^{223}Ra: 9±0.9 and 14±1.4 cm/d, respectively) and spring 2017 (all bay average of ^{226}Ra and ^{223}Ra: 14±1.4 and 10±1.0 cm/d, respectively). The highest average SGD rate across all bays was determined for winter 2018 (all bay average of ^{226}Ra and ^{223}Ra: 26±2.6 and 45±4.5 cm/d, respectively).

This observed variability in radium SGD rates is mainly related to changes in the porewater and surface water activities (**Table 7; Table 8**) as they influence the water ages, the ^{226}Ra inventory, and the conversion to a final bay wide SGD (Charette et al. 2001). Available porewater ^{224}Ra and ^{223}Ra show a significant increase in activities from winter 2017 to spring and summer 2017. On the other hand, average ^{226}Ra activities across all bays are gradually decreasing from winter 2017 to winter 2018. Because of these differences in porewater radium activities, the resulting SGD is different, especially in winter 2017. Depending on the surface water activities, these SGD estimates will also vary. For instance, in winter 2017, the^{224}Ra and ^{223}Ra activities are more elevated in porewater than they are in surface water, comparative to the other seasons. This leads to larger SGD rates derived using the radium-223 activity. However, despite larger surface water activities in spring 2017, because the porewater activities also increased, SGD rates are much lower than in winter 2017.

Differences in the two radium isotope SGD estimates (using the ^{223}Ra and ^{226}Ra activity of porewater and the ^{224}Ra/^{223}Ra activity ratios of surface water), also result from their different

inputs and response to salinity effects. For instance, radium desorption from sediments is expected to reach a maximum at an approximately salinity of 20 (Elsinger and Moore 1980; Webster et al. 1995), with positive relationships between salinity and the radioisotopes. As noted earlier, there is a salinity gradient from north to south, not only in porewater but surface water. While radon is unreactive and produces estimates of total SGD (including fresh and saline terrestrial groundwater and recirculating seawater) (Burnett and Dulaiova 2003), salinity-dependent radium may only provide the saline portion of SGD (recirculated seawater and saline terrestrial inputs) and underestimates the fresher component (Moore 2006). This is mostly expected when ^{226}Ra is used as the groundwater tracer as, given its longer half-life and time require to reach secular equilibrium are longer, when compared to the short-lived ^{224}Ra and ^{223}Ra.

Table 13. Correlation between salinity and ^{223}Ra, ^{224}Ra and ^{226}Ra in surface water.

	Dec 2016 - Jan 2017 (winter 2017)		April - June 2017 (spring 2017)		August - Sep 2017 (summer 2017)		Dec 2017 - Jan 2018 (winter 2018)	
	r	p	r	p	r	p	r	p
^{223}Ra	-0.75	**<0.01**	0.09	0.72	-0.15	0.59	-0.39	0.11
^{224}Ra	-0.73	**<0.01**	0.18	0.47	-0.40	0.14	-0.24	0.35
^{226}Ra	0.56	0.02	0.69	**<0.01**	0.65	**0.01**	0.46	0.06

As indicated by the response of ^{226}Ra to salinity changes across all systems, the only significant relationship is observed in spring and summer 2017, and only in surface water (**Table 13; Table 14).** ^{223}Ra and ^{224}Ra show a negative correlation with salinity in winter 2017 in surface water and porewater and, similar to ^{226}Ra, a positive correlation only for ^{224}Ra in spring and summer 2017. A negative correlation between salinity and radium indicates in winter 2017, the seasons with one of the lowest overall salinities, in both pore- and surface-water (34 and 31, respectively) likely indicates that salinity does not necessarily play a role in the observed

changes in radium. The same applies to winter 2018, although correlations are not significant at the 99% confidence.

Table 14. Correlation between salinity and ^{223}Ra, ^{224}Ra and ^{226}Ra in porewater and dug-well.

	Dec 2016 - Jan 2017 (winter 2017)		April - June 2017 (spring 2017)		August - Sep 2017 (summer 2017)		Dec 2017 - Jan 2018 (winter 2018)	
	r	p	r	p	r	p	r	p
^{223}Ra	-0.63	**0.01**	0.54	0.01	-0.05	0.86	-0.06	0.76
^{224}Ra	-0.68	**0.01**	0.69	**<0.01**	0.99	**<0.01**	-0.06	0.78
^{226}Ra	0.56	0.06	0.37	0.12	0.40	0.14	0.03	0.89

Lower radium SGD rates when compared to radon-derived rates as observed in winter 2017, across all bays, and in Aransas Bay, Nueces Bay and University Beach across all seasons are indicative of low saline inputs. In Laguna Madre the radium and radon rates agree well across all seasons when the mid-value for radon-derived SGD is considered. In this system, porewater radon activities are consistently very low, thus SGD rates derived using this endmember result in large SGD rates. There are two instances where radium-derived SGD exceed those calculated from radon **(Table 10; Table 14)**. Summer 2017 in Baffin Bay exhibit larger than expected ^{223}Ra-derived SGD rates, when the highest porewater salinity was also measured. Similarly, in winter 2018 Oso Bay ^{223}Ra and ^{226}Ra SGD rates are more than double the highest possible radon rates. In Baffin Bay large production of radium in porewater during the hot, dry summer months was observed before (Lopez et al. 2018), thus larger saline inputs may be expected; however, only if the advective SGD is also higher. In Oso Bay, there is no historical data to compare to and the porewater salinity does not explain an increase in radium activities, unless there is additional lateral subsurface input. While in these two systems saline input from groundwater, these inputs are not captured by the total SGD estimates (i.e., radon

SGD). Therefore, it is likely that the groundwater endmember (i.e., porewater) or the offshore inputs are not well constrained.

Nutrient Fluxes

Groundwater-derived nutrient fluxes were calculated using the radon-derived SGD rates calculated using the regional groundwater average radon endmember. Groundwater discharge rates vary slightly by season at most locations, but no preferential seasonal trend was identified. The average of SGD rates across all bays exhibited very little change between winter 2017 (51 cm/d), spring 2017 (45 cm/d), summer (69 cm/d) and winter 2018 (69 cm/d). Furthermore, nutrient concentrations measured in the interstitial porewater also vary spatially and temporally, but tend to follow a similar seasonal and spatial trend **(Figure 5; Figure 6).**

The estimates suggest that SGD delivers significant amounts of nitrate in Oso and Baffin bays, in summer 2017 and winter 2018 (all seasons average: $65.6*10^3$ and $5.3*10^3$ μmol/m^2/day, respectively). The largest flux however, occurred in Oso Bay in winter 2017 **(Figure 11A)**, a result of higher nitrate concentrations **(Figure 6)** and slightly more elevated SGD rates **(Figure 8)**. In Baffin Bay, the fluxes are lower than in Oso Bay because of lower SGD rates and slightly lower nitrate concentrations such as for winter 2017. All other locations, except for Nueces Bay, exhibit average nitrate fluxes lower than $1*10^3$ μmol/m^2/day. Average rates in Nueces Bay are $1.2*10^3$ μmol/m^2/day. As expected, nitrite SGD fluxes are lower when compared to nitrate but they follow the same trend **(Figure 11A, B).**

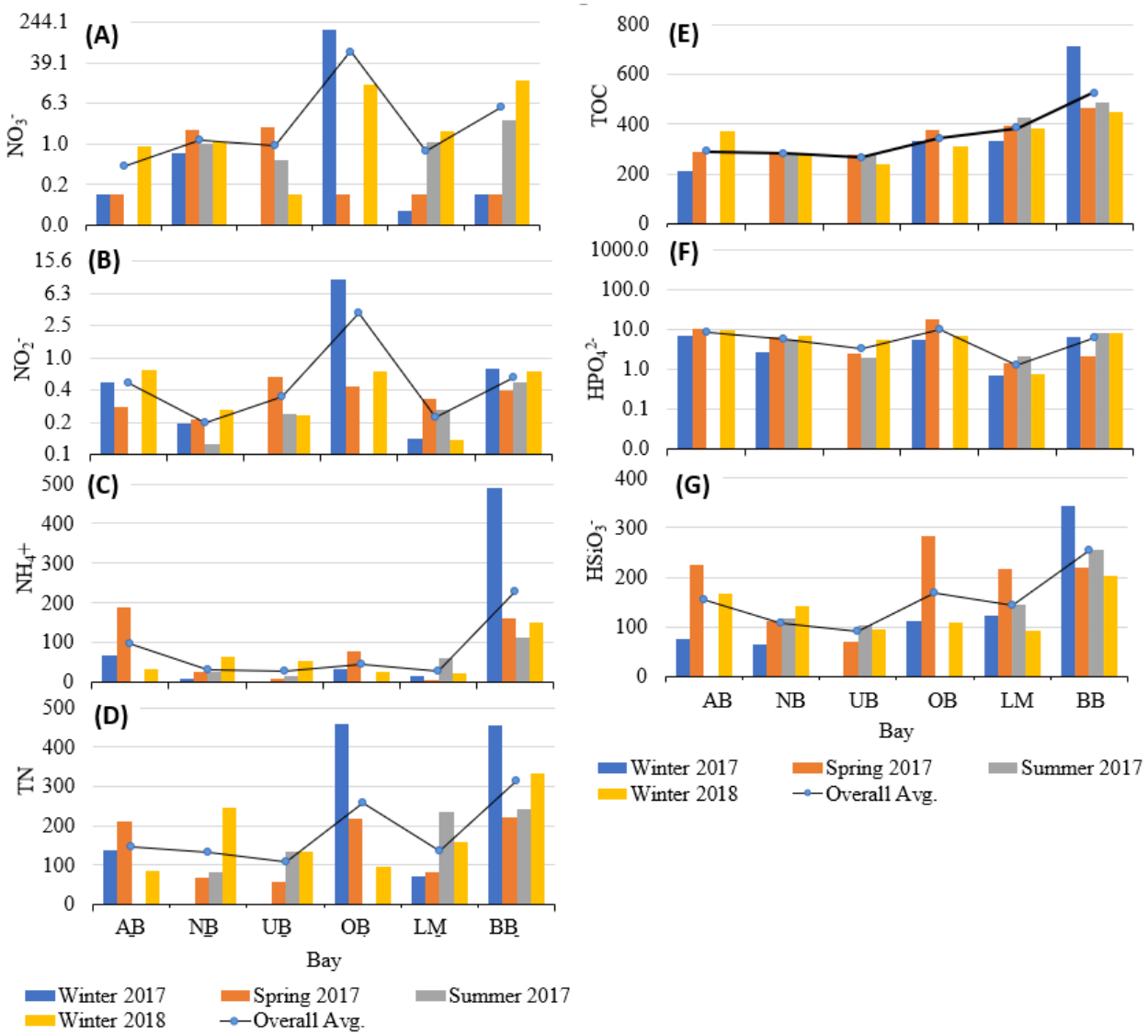

Figure 11. Nutrient flux rates for selected constituents are presented in $\cdot 10^3$ µmol/m^2/d for the bays of interest.

Table 15. Nutrient Flux Rates for selected constituents are presented in $\cdot 10^3$ µmol/m^2/d for the bays of interest with the minimum and maximum flux rate determined using the highest and lowest porewater concentrations for each sampling event and bay. Values in red text were calculated using the average porewater concentration for the station. † Winter 2017 NB samples were collected from station 7 from Murgulet et. al. (2018). ‡ Winter 2017 BB samples are from station 11 from Lopez et. al. (2018).

		AB			NB†			UB			OB			LM			BB‡		
		Min.	Max.	Avg.	Min.	Max.	Avg.	Min.	Max.	Avg.	Min.	Max.	Avg.	Min.	Max.	Avg.	Min.	Max.	Avg.
December 2016 - January 2017	NO_3	2.4	2.4	2.4	27.9	120.8	74.8	12.7	59.8	31.4	8,773	19,726	13,322	1.6	2.6	0.8	4.2	4.2	4.2
	NO_2	8.4	15.1	11.8	1.3	53.6	17.8	8.9	14.9	11.4	350.0	933.2	685.0	0.2	2.7	1.6	28.8	32.1	30.9
	NH_4	1,156	2,015	1,567	652	1,243	852	591	1,213	934	1,296	3,375	2,455	54	474	262	20,191	20,800	20,481
	HPO_4	138.6	180.5	159.8	293.3	338.3	309.9	93.7	129.3	115.5	173.4	552.8	406.9	7.5	14.2	10.8	211.7	288.2	259.6
	$HSiO_3$	1,128	2,275	1,764	5,303	8,714	7,562	2,775	3,477	3,157	7,161	9,155	8,164	1,710	2,036	1,892	10,811	15,878	14,483
	Urea	30.3	53.0	39.3	8.5	311.7	122.9	21.4	36.7	27.3	47.5	82.3	68.2	6.8	8.6	7.3	93.2	121.9	106.5
	TOC	4,092	5,858	4,975	29,916	34,489	32,455	8,720	9,939	9,280	22,132	27,151	24,429	4,355	5,965	5,160	25,020	34,538	30,000
	TN	2,506	3,999	3,252	12,489	10,834	15,291	3,175	4,300	3,847	26,787	42,834	33,510	662	1,534	1,098	18,402	19,696	19,141
April - June 2017	NO_3	1.6	1.6	1.6	130.5	268.5	180.1	70.9	263.8	167.4			5.6	1.4	1.4	1.4	0.6	0.6	0.6
	NO_2	1.8	5.5	3.8	9.4	30.0	16.3	36.8	56.6	46.7			24.4	4.0	5.0	4.4	2.3	2.7	2.5
	NH_4	2,686	3,150	2,932	1,244	3,473	2,444	759	767	763			4,231	63	109	89	970	1,088	1,004
	HPO_4	141.0	164.1	154.0	315.0	825.7	611.6	177.9	226.3	202.1			979.5	18.6	22.5	20.4	12.2	13.1	12.8
	$HSiO_3$	3,270	3,865	3,486	9,739	11,519	10,624	5,545	5,624	5,585			15,772	2,748	3,357	3,060	1,245	1,478	1,370
	Urea	8.0	11.9	9.3	27.0	48.3	35.9	62.0	82.5	72.2			74.0	15.3	17.6	16.4	7.1	8.2	7.8
	TOC	4,050	5,241	4,453	22,186	32,332	26,857	20,397	23,881	22,139			20,992	5,381	5,672	5,527	2,811	2,961	2,907
	TN	3,214	3,427	3,316	5,398	8,112	6,614	4,230	5,050	4,640			12,222	1,036	1,290	1,163	1,287	1,498	1,401
August - September 2017	NO_3	Goose Island State Park closed due to Hurricane Harvey damage.			157.2	166.1	162.8	7.9	135.4	38.8	2,741	6,420	4,303	34.7	40.5	37.6	13.3	25.6	19.5
	NO_2				11.3	16.3	13.7	12.3	21.8	15.7	123.2	310.4	229.8	7.8	8.8	8.3	2.6	4.0	3.3
	NH_4				4,048	5,006	4,370	1,037	1,562	1,262	2,526	3,320	2,959	555	3,699	2,127	668	827	748
	HPO_4				482.2	1,163.6	878.9	130.7	158.4	147.5	530.7	762.2	659.6	71.6	81.1	76.4	50.0	61.2	55.6
	$HSiO_3$				12,412	26,499	18,353	7,635	8,921	8,214	10,485	11,547	11,018	4,795	5,528	5,162	1,580	1,796	1,688
	Urea				28.0	142.5	67.1	35.7	92.3	56.3	55.7	67.8	62.8	19.1	23.0	21.1	7.2	7.7	7.5
	TOC				43,297	46,264	44,547	21,595	22,568	22,007	20,913	24,037	22,412	14,628	16,196	15,412	3,205	3,246	3,226
	TN				12,185	15,351	13,283	10,041	11,475	10,622	14,866	19,822	16,954	2,831	14,211	8,521	1,470	1,735	1,602
December 2017 - January2018	NO_3	31.6	47.5	39.5	65.4	80.1	71.3	23.3	23.3	23.3	255.8	1,176.4	716.1	20.2	22.6	21.4	10.0	153.9	82.6
	NO_2	31.3	32.7	32.0	13.9	16.5	15.2	33.5	67.5	45.0	20.2	49.2	34.7	0.7	1.7	1.2	2.1	4.2	3.1
	NH_4	1,438	1,609	1,523	3,162	5,526	4,342	6,493	17,285	12,634	1,098	1,496	1,297	292	294	293	593	769	690
	HPO_4	353.8	501.7	427.7	433.3	536.3	477.4	960.2	1,447.1	1,275.2	217.0	490.6	353.8	7.6	11.2	9.4	25.7	46.9	35.8
	$HSiO_3$	7,460	7,493	7,476	9,282	9,737	9,456	16,522	26,452	22,286	4,957	6,037	5,497	1,018	1,233	1,126	881	973	931
	Urea	76.1	78.2	77.2	35.1	31.7	37.2	140.3	218.2	167.5	28.7	32.7	30.7	1.9	4.1	3.0	7.9	11.6	9.6
	TOC	11,694	21,626	16,660	18,293	17,933	18,928	50,344	61,604	55,213	13,990	17,753	15,871	4,468	4,806	4,637	2,018	2,111	2,070
	TN	3,768	3,812	3,790	12,787	6,709	16,338	21,169	36,942	31,636	4,716	5,057	4,887	1,177	2,678	1,927	1,464	1,575	1,527

The most elevated ammonium fluxes were calculated for Baffin Bay followed by Aransas Bay (all seasons average: $227.8*10^3$ and $96.3*10^3$ μmol/m^2/day, respectively). Fluxes for all other locations are lower by one order of magnitude when compared to Baffin Bay and about three times lower than Aransas Bay **(Figure 11C**).

Fluxes of TN seem to be influenced more by the nitrate+nitrite concentration profiles of each bay as the trend of average fluxes are similar **(Figure 11D**). Concentrations of DON were not measured in porewater; thus, SGD fluxes are not available. However, as with porewater porewater, the total of nitrate+nitrite+ammonium (DIN) is lower than the TN, thus, the difference is likely to be attributed to DON. In surface water DON seasonal concentration profiles are changing from Aransas Bay to Baffin Bay which likely reflects the different magnitude of inputs. Like the surface water concentrations of DON, the difference between the DIN and TN fluxes is also increasing from Aransas Bay to Baffin Bay **(Figure 11D**).

Similar to surface water and porewater TOC concentration profiles across the north to south climatic gradient, SGD-derived TOC fluxes also show an increase from the semi-wet Aransas Bay to the semi-dry Baffin Bay **(Figure 11E**). Fluxes rates in Baffin Bay are almost twice as high as in Aransas Bay (seasons average: $529.1*10^3$ and $290.1*10^3$ μmol/m^2/d, respectively). In addition, both silica and phosphate fluxes are like concentration trends in porewater and surface water **(Figure 5; Figure 6; Figure 11)**. For instance, the largest overall phosphate fluxes were estimated Oso Bay (seasons average: $10.1*10^3$ μmol/m^2/d) and the lowest in Laguna Madre (seasons average: $1.3*10^3$ μmol/m^2/d). The largest silica fluxes occurred in Baffin Bay (seasons average: $255.3*10^3$ μmol/m^2/d) and the lowest at the University Beach (seasons average: $90*10^3$ μmol/m^2/d).

SUMMARY

The main purpose of this study is to advance understanding of groundwater inflows and nutrient transport to bay systems in South Texas (i.e., Aransas Bay, Nueces Bay, Corpus Christi Bay at University Beach, Oso Bay, Upper Laguna Madre and Baffin bay) for improved Environmental Flow recommendations and nutrient criteria by explicitly incorporating groundwater discharge into the freshwater inflow needs and nutrient budgets to the south Texas coastal embayments. Specifically, this project builds recent efforts to estimate freshwater and nutrient contributions from groundwater to the Nueces River, Laguna Madre, and Baffin Bay estuaries (projects underway).

Measured surface water dissolved organic nitrogen (DON) concentrations show an increase from Aransas Bay to Baffin Bay. While DON follows an increasing gradient from north to south, dissolved inorganic nitrogen (DIN) concentrations show a different pattern. Most nitrate concentrations throughout the bays and seasons are consistently below 2.5 μM. However, significantly higher concentrations of nitrate were measured in Oso Bay in the winter 2017 and 2018 seasons (i.e., max: 72.5 and 139.6 μM, respectively). Ammonium concentrations were less than 10 μM across all bays and seasons with the highest concentrations measured in summer 2017 and winter 2018 in Baffin Bay (p.6 and 9.4 μM, respectively), which also exhibited the highest of all season's average concentrations (7.9 μM). Oso Bay has the second highest overall average of ammonium (5.1 μM).

The largest submarine groundwater discharge (SGD) rates occurred in Nueces Bay and at the University Beach (seasons average: 109 and 107 cm/d, respectively) while the lowest occurred in Baffin Bay, Laguna Madre and Aransas Bay (seasons average: 15, 19 and 28 cm/d,

respectively). Oso Bay rates are very similar across seasons ranging from 56 cm/d (spring 2017) to 73 cm/d in winter 2017. The highest SGD rate among all bays was measured in winter 2018 at University Beach (233 cm/d). In winter 2018, a higher SGD, when compared to other seasons, was measured in Aransas Bay (44.7 cm/d), but the rate is smaller than any of the ones measured in Nueces Bay and University Beach and approaching the one in Oso Bay (50.8 cm/d). Based on quarterly continuous measurements of SGD during approximately 24-hours, or less, there was no strong evidence of a seasonal fluctuation that applies across all bays. However, monthly monitoring of SGD at the University Beach indicates that SGD rates are responding to climatic conditions, with the largest SGD rates measured during the wet fall-winter months and the lowest during the driest summer months.

Subsurface solute fluxes suggest that SGD delivers significant amounts of nitrate in Oso and Baffin bays, summer 2017 and winter 2018 (all seasons average: $65.6*10^3$ and $5.3*10^3$ $\mu mol/m^2/day$, respectively). The largest flux however, occurred in Oso Bay in winter 2017, a result of more elevated nitrate concentrations and slightly more elevated SGD rates. In Baffin Bay, the fluxes are lower than in Oso Bay because of lower SGD rates and slightly lower nitrate concentrations such as for winter 2017. All other locations, except for Nueces Bay, exhibit average nitrate fluxes lower than $1*10^3$ $\mu mol/m^2/day$. Average rates in Nueces Bay are $1.2*10^3$ $\mu mol/m^2/day$. Nitrite fluxes show a similar trend to nitrate but are much lower. The most elevated ammonium fluxes were calculated for Baffin Bay followed by Aransas Bay (all seasons average: $227.8*10^3$ and $96.3*10^3$ $\mu mol/m^2/day$, respectively). Fluxes for all other locations are lower by one order of magnitude when compared to Baffin Bay and about three times lower than

Aransas Bay. Fluxes of TN seem to be influenced more by the nitrate+nitrite concentration profiles of each bay as the trend of average fluxes are similar.

SGD-derived TOC fluxes follow a similar pattern as the surface water and porewater TOC concentrations which increase across the north to south climatic gradient; fluxes rates in Baffin Bay are almost twice as high as in Aransas Bay (seasons average: $529.1*10^3$ and $290.1*10^3$ μmol/m^2/d, respectively). In addition, both silica and phosphate fluxes are similar to concentration trends in porewater and surface water. Oso Bay exhibited the largest overall phosphate fluxes (seasons average: $10.1*10^3$ μmol/m^2/d) while Laguna Madre the lowest (seasons average: $1.3*10^3$ μmol/m^2/d). For silica, the largest silica fluxes occurred Baffin Bay (seasons average: $255.3*10^3$ μmol/m^2/d) and the lowest at the University Beach (seasons average: $90*10^3$ μmol/m^2/d).

As observed in this study, overall the largest nutrient fluxes bounce between Oso and Baffin bays, which had consistently the highest Chl-a levels across all seasons. The only exception is winter 2018 when Aransas Bay has similar concentrations. Thus, the nutrient input associated with sediment benthic fluxes should not be ignored, particularly in these two bays which have shown to be impacted by significant water quality degradation.

REFERENCES

Alexander, H. D. & K. H. Dunton, 2006. Treated wastewater effluent as an alternative freshwater source in a hypersaline salt marsh: Impacts on salinity, inorganic nitrogen, and emergent vegetation. J Coastal Res 22(2):377-392 doi:10.2112/04-0234.1.

An, S. & W. S. Gardner, 2000. Nitrogen cycling in Laguna Madre and Baffin Bay.

Armstrong, N. E., M. S. Brody, N. Funicelli & National Wetlands Research Center (U.S.), 1987. The ecology of open-bay bottoms of Texas : a community profile. U.S. Dept. of the Interior, Fish and Wildlife Service, Research and Development, National Wetlands Research Center, Washington, DC.

Ashworth, J. B. & J. Hopkins, 1995. Major and minor aquifers of Texas. In: Board, T. W. D. (ed). 69 p.

Baker, E. T., 1979. Stratigraphic and Hydrogeologic Framework of Part of the Coastal Plain of Texas.

Bighash, P. & D. Murgulet, 2015. Application of factor analysis and electrical resistivity to understand groundwater contributions to coastal embayments in semi-arid and hypersaline coastal settings. Sci Total Environ 532:688-701 doi:10.1016/j.scitotenv.2015.06.077.

Bowen, G. J., A. Putman, J. R. Brooks, D. R. Bowling, E. J. Oerter & S. P. Good, 2018. Inferring the source of evaporated waters using stable H and O isotopes. Oecologia 187(4):1025-1039.

Boyd, P. W., A. J. Watson, C. S. Law, E. R. Abraham, T. Trull, R. Murdoch, D. C. Bakker, A. R. Bowie, K. Buesseler & H. Chang, 2000. A mesoscale phytoplankton bloom in the polar Southern Ocean stimulated by iron fertilization. Nature 407(6805):695-702.

Breier, J. A., C. F. Breier & H. N. Edmonds, 2010. Seasonal dynamics of dissolved Ra isotopes in the semi-arid bays of south Texas. Mar Chem 122(1-4):39-50.

Brown, R. M., N. I. McClelland, R. A. Deininger & R. G. Tozer, 1970. A WATER QUALITY INDEX- DO WE DARE.

Burnett, W. C., 2003. Radon and radium isotopes as tracers in the coastal ocean. Abstr Pap Am Chem S 226:U81-U81.

Burnett, W. C. & H. Dulaiova, 2003. Estimating the dynamics of groundwater input into the coastal zone via continuous radon-222 measurements. J Environ Radioactiv 69(1-2):21-35.

Burnett, W. C., M. Taniguchi & J. Oberdorfer, 2001. Measurement and significance of the direct discharge of groundwater into the coastal zone. J Sea Res 46(2):109-116.

Cable, J. E., J. B. Martin, P. W. Swarzenski, M. K. Lindenberg & J. Steward, 2004. Advection Within Shallow Pore Waters of a Coastal Lagoon, Florida. Ground Water 42(7):1011-1020 doi:10.1111/j.1745-6584.2004.tb02640.x.

Cardenas, M. B., P. B. Zamora, F. P. Siringan, M. R. Lapus, R. S. Rodolfo, G. S. Jacinto, M. L. San Diego-McGlone, C. L. Villanoy, O. Cabrera & M. I. Senal, 2010. Linking regional sources and pathways for submarine groundwater discharge at a reef by electrical resistivity tomography, Rn-222, and salinity measurements. Geophys Res Lett 37 doi:Artn L16401 10.1029/2010gl044066.

CBI (Conrad Blucher Institute for Surveying and Science), 2019. Stations. In: DNR (Division of Nearshore Research). http://cbi.tamucc.edu/dnr/station/ Accessed September 10.

Cech, I., C. Kreitler, H. Prichard, A. Holguin & M. Lemma, 1988. Radon Distribution in Domestic Water of Texas. Ground Water 26(5):561-569 doi:10.1111/j.1745-6584.1988.tb00789.x.
Cerdà-Domènech, M., V. Rodellas, A. Folch & J. Garcia-Orellana, 2017. Constraining the temporal variations of Ra isotopes and Rn in the groundwater end-member: Implications for derived SGD estimates. Science of the total environment 595:849-857.
Charette, M. A., K. O. Buesseler & J. E. Andrews, 2001. Utility of radium isotopes for evaluating the input and transport of groundwater-derived nitrogen to a Cape Cod estuary. Limnology and Oceanography 46(2):465-470.
Church, T. M., 1996. An underground route for the water cycle. Nature 380(6575):579-580 doi:DOI 10.1038/380579a0.
Corbett, D. R., W. C. Burnett, P. H. Cable & S. B. Clark, 1998. A multiple approach to the determination of radon fluxes from sediments. J Radioanal Nucl Ch 236(1-2):247-252.
Cyronak, T., I. R. Santos, D. V. Erler & B. D. Eyre, 2013. Groundwater and porewater as major sources of alkalinity to a fringing coral reef lagoon (Muri Lagoon, Cook Islands). Biogeosciences 10(4):2467-2480 doi:10.5194/bg-10-2467-2013.
Dimova, N., W. C. Burnett, E. P. Horwitz & D. Lane-Smith, 2007. Automated measurement of Ra-224 and Ra-226 in water. Appl Radiat Isotopes 65(4):428-434.
Dimova, N. T., W. C. Burnett, J. P. Chanton & J. E. Corbett, 2013. Application of radon-222 to investigate groundwater discharge into small shallow lakes. Journal of Hydrology 486:112-122.
Dortch, Q., 1990. The Interaction between Ammonium and Nitrate Uptake in Phytoplankton. Mar Ecol Prog Ser 61(1-2):183-201 doi:10.3354/meps061183.
Douglas, A., D. Murgulet, M. S. Wetz & N. Spalt, 2017. Evaluating Groundwater Inflow and Nutrient Transport to Texas Coastal Embayments Phase II. Texas General Land Office, Texas General Land Office.
Elsinger, R. J. & W. S. Moore, 1980. 226Ra behavior in the pee Dee River-Winyah Bay estuary. Earth and Planetary Science Letters 48(2):239-249.
Garcia-Orellana, J., V. Rodellas, N. Casacuberta, E. Lopez-Castillo, M. Vilarrasa, V. Moreno, E. Garcia-Solsona & P. Masque, 2013. Submarine groundwater discharge: Natural radioactivity accumulation in a wetland ecosystem. Mar Chem 156:61-72 doi:10.1016/j.marchem.2013.02.004.
Grossman, E. L., L. A. Cifuentes & I. M. Cozzarelli, 2002. Anaerobic methane oxidation in a landfill-leachate plume. Environ Sci Technol 36(11):2436-42 doi:10.1021/es015695y.
Guo, W. & C. D. Langevin, 2002. User's guide to SEAWAT; a computer program for simulation of three-dimensional variable-density ground-water flow Techniques of Water-Resources Investigations. Supersedes OFR 01-434 edn.
Harred, L. B. & L. Campbell, 2014. Predicting harmful algal blooms: a case study with Dinophysis ovum in the Gulf of Mexico. Journal of Plankton Research:fbu070.
Henderson, A. K. & B. N. Shuman, 2010. Differing controls on river-and lake-water hydrogen and oxygen isotopic values in the western United States. Hydrological Processes 24(26):3894-3906.
Kattner, G., 1999. Storage of dissolved inorganic nutrients in seawater: poisoning with mercuric chloride. Mar Chem 67(1-2):61-66 doi:Doi 10.1016/S0304-4203(99)00049-3.

Katz, B. G., T. B. Coplen, T. D. Bullen & J. H. Davis, 1997. Use of chemical and isotopic tracers to characterize the interactions between ground water and surface water in mantled karst. Ground Water 35(6):1014-1028 doi:10.1111/j.1745-6584.1997.tb00174.x.

Kendall, C. & J. J. McDonnell, 2012. Isotope tracers in catchment hydrology. Elsevier.

Khan, S. & A. R. Kumar, 2012. Interpretation of Groundwater Quality using Correlation and Linear Regression Analysis from Tiruchengode taluk, Namakkal district, Tamilnadu, India. Journal of Chemical and Pharmaceutical Research 4(10):4514-4521.

Kim, G., W. C. Burnett, H. Dulaiova, P. W. Swarzenski & W. S. Moore, 2001. Measurement of Ra-224 and Ra-226 activities in natural waters using a radon-in-air monitor. Environmental Science & Technology 35(23):4680-4683.

Kim, H. C. & P. A. Montagna, 2012. Effects of climate-driven freshwater inflow variability on macrobenthic secondary production in Texas lagoonal estuaries: A modeling study. Ecol Model 235:67-80 doi:10.1016/j.ecolmodel.2012.03.022.

Knee, K. L., E. Garcia-Solsona, J. Garcia-Orellana, A. B. Boehm & A. Paytan, 2011. Using radium isotopes to characterize water ages and coastal mixing rates: A sensitivity analysis. Limnol Oceanogr-Meth 9:380-395 doi:10.4319/lom.2011.9.380.

Lamontagne, S., C. L. G. La Salle, G. J. Hancock, I. T. Webster, C. T. Simmons, A. J. Love, J. James-Smith, A. J. Smith, J. Kämpf & H. J. Fallowfield, 2008. Radium and radon radioisotopes in regional groundwater, intertidal groundwater, and seawater in the Adelaide Coastal Waters Study area: implications for the evaluation of submarine groundwater discharge. Mar Chem 109(3):318-336.

Lebreton, B., J. B. Pollack, B. Blomberg, T. A. Palmer, L. Adams, G. Guillou & P. A. Montagna, 2016. Origin, composition and quality of suspended particulate organic matter in relation to freshwater inflow in a South Texas estuary. Estuar Coast Shelf S 170:70-82 doi:10.1016/j.ecss.2015.12.024.

Longley, W. L., G. L. Powell, A. W. Green & T. W. D. Board, 1994. Freshwater inflows to Texas bays and estuaries: ecological relationships and methods for determination of needs. Texas Water Development Board, Austin, TX.

Lopez, C., D. Murgulet, A. Douglas & V. Murgulet, 2018. Impacts of Temporal and Spatial Variation of Submarine Groundwater Discharge on Nutrient Fluxes to Texas Coastal Embayments, Phase III (Baffin Bay). 105.

Mace, R. E., W. F. Mullican, E. S. Angle, S. C. Davidson & Texas Water Development Board., 2006. Aquifers of the Gulf coast of Texas. Texas Water Development Board, Austin, Tex.

Montagna, P. A. & C. Ritter, 2006. Direct and indirect effects of hypoxia on benthos in Corpus Christi Bay, Texas, USA. J Exp Mar Biol Ecol 330(1):119-131 doi:10.1016/j.jembe.2005.12.021.

Mooney, R. F. & J. W. McClelland, 2012. Watershed Export Events and Ecosystem Responses in the Mission-Aransas National Estuarine Research Reserve, South Texas. Estuar Coast 35(6):1468-1485 doi:10.1007/s12237-012-9537-4.

Moore, W. S., 1996. Large groundwater inputs to coastal waters revealed by Ra-226 enrichments. Nature 380(6575):612-614 doi:DOI 10.1038/380612a0.

Moore, W. S., 2006. Radium isotopes as tracers of submarine groundwater discharge in Sicily. Continental Shelf Research 26(7):852-861 doi:http://dx.doi.org/10.1016/j.csr.2005.12.004.

Morehead, S., P. Montagna & M. C. Kennicutt, 2008. Comparing fixed-point and probabilistic sampling designs for monitoring the marine ecosystem near McMurdo Station, Ross Sea, Antarctica. Antarct Sci 20(5):471-484 doi:10.1017/S0954102008001326.

Morell, I., E. Gimenez & M. V. Esteller, 1996. Application of principal components analysis to the study of salinization on the Castellon Plain (Spain). Science of the Total Environment 177:161-171 doi:10.1016/0048-9697(95)04893-6.

Morton, R. A. & J. McGowen, 1980. Modern depositional environments of the Texas coast. University of Texas at Austin, Bureau of Economic Geology.

Murgulet, D. & G. R. Tick, 2016. Effect of variable-density groundwater flow on nitrate flux to coastal waters. Hydrological Processes 30(2):302-319 doi:10.1002/hyp.10580.

Murgulet, D., M. Trevino, A. Douglas, N. Spalt, X. Hu & V. Murgulet, 2018. Temporal and spatial fluctuations of groundwater-derived alkalinity fluxes to a semiarid coastal embayment. Science of The Total Environment 630:1343-1359 doi:https://doi.org/10.1016/j.scitotenv.2018.02.333.

Murgulet, D., M. S. Wetz, A. Douglas, W. McBee, N. Spalt & K. Linares, 2015. Evaluating Groundwater Inflow and Nutrient Transport to Texas Coastal Embayments. Texas General Land Office.

Nelson, K. & P. A. Montagna, 2009. Causes and Monitoring of Hypoxia in Corpus Christi Bay.

NOAA (National Oceanic and Atmospheric Administration), 2014. National Weather Service. In. https://www.ncdc.noaa.gov/.

NOAA (National Oceanic and Atmospheric Administration), 2019. Daily Summaries. In: National Climate Data Center, Climate Data Online. https://www.ncdc.noaa.gov/cdo-web/datatools/findstation Accessed September 10.

Nyquist, J. E., P. A. Freyer & L. Toran, 2008. Stream bottom resistivity tomography to map ground water discharge. Ground Water 46(4):561-9 doi:10.1111/j.1745-6584.2008.00432.x.

Palmer, T. A., P. A. Montagna, J. B. Pollack, R. D. Kalke & H. R. DeYoe, 2011. The role of freshwater inflow in lagoons, rivers, and bays. Hydrobiologia 667(1):49-67 doi:10.1007/s10750-011-0637-0.

Peterson, R. N., W. C. Burnett, M. Taniguchi, J. Chen, I. R. Santos & T. Ishitobi, 2008. Radon and radium isotope assessment of submarine groundwater discharge in the Yellow River delta, China. Journal of Geophysical Research 113(C9) doi:10.1029/2008jc004776.

Quammen, M. L. & C. P. Onuf, 1993. Laguna Madre: seagrass changes continue decades after salinity reduction. Estuaries 16(2):302-310.

RCRA SOP, 2009. Protocol for Groundwater/Surface Water Interface Sampling Using a Pore Water Sampler. In: Beneski, B. & E. Bonenfant (eds) Standard Operating Procedure Change Record. Department of Environmental Protection Bureau of Remediation and Waste Management RCRA Program.

Schmidt, D. H. & K. A. Garland, 2012. Bone Dry in Texas: Resilience to Drought on the Upper Texas Gulf Coast. J Plan Lit 27(4):434-445 doi:10.1177/0885412212454013.

Spalt, N., D. Murgulet & X. Hu, 2018. Relating estuarine geology to groundwater discharge at an oyster reef in Copano Bay, TX. Journal of hydrology 564:785-801.

Su, N., W. C. Burnett, K. T. Eller, H. L. MacIntyre, B. Mortazavi, J. D. Liefer & L. Novoveská, 2012. Radon and radium isotopes, groundwater discharge and harmful algal blooms in Little Lagoon, Alabama. Interdisciplinary studies on environmental chemistry 6:329-337.

Sun, Y. & T. Torgersen, 1998. The effects of water content and Mn-fiber surface conditions on Ra-224 measurement by Rn-220 emanation. Mar Chem 62(3-4):299-306.
Swarzenski, P. W., C. Reich, K. D. Kroeger & M. Baskaran, 2007. Ra and Rn isotopes as natural tracers of submarine groundwater discharge in Tampa Bay, Florida. Mar Chem 104(1):69-84.
Thareja, S., S. Choudhury & P. Trivedi, 2011. Assessment of water quality of Ganga River in Kanpur by using principal components analysis. Adv Appl Sci Res 2(5):84-91.
TWDB (Texas Water Development Board), 2016. Hydrology for the Laguna Madre Estuary Watershed. In: Studies, C. f. W. S. (ed). Freshwater Inflow Estimates.
TWDB (Texas Water Development Board), 2017. Mission-Aransas Estuary. In: Bays & Estuaries. http://www.twdb.texas.gov/surfacewater/bays/major_estuaries/mission_aransas/ Accessed March 2017.
TWDB (Texas Water Development Board), 2019. Freshwater Inflow Estimates. In: Water Data for Texas: Coastal. Available via Texas Water Development Board. https://waterdatafortexas.org/coastal/hydrology.
Urquidi-Gaume, M., I. R. Santos & C. Lechuga-Deveze, 2016. Submarine groundwater discharge as a source of dissolved nutrients to an arid coastal embayment (La Paz, Mexico). Environmental Earth Sciences 75(2):1.
USDA (U.S. Department of Agriculture and Natural Resources Conservation Service), 2012. National Soil Survey Handbook, Title 430-VI. In. http://www.nrcs.usda.gov/wps/portal/nrcs/detail/soils/ref/?cid=nrcs142p2_054242 Accessed April 2012.
USGS (U.S. Geological Survey), 2019. Daily Data for Texas. In: National Water Information System: Surface Water. https://nwis.waterdata.usgs.gov/tx/nwis/dv Accessed September 10.
Voudouris, K., A. Panagopoulos & J. Koumantakis, 2000. Multivariate statistical analysis in the assessment of hydrochemistry of the northern Korinthia prefecture alluvial aquifer system (Peloponnese, Greece). Natural Resources Research 9(2):135-146.
Waterstone & Parsons, 2003. Groundwater availability of the central Gulf Coast aquifer--Numerical simulations to 2050, Central Gulf Coast, Texas.
Webster, I. T., G. J. Hancock & A. S. Murray, 1995. Modelling the effect of salinity on radium desorption from sediments. Geochimica et Cosmochimica Acta 59(12):2469-2476.
Wood, W. W., 1976. Guidelines for collection and field analysis of ground-water samples for selected unstable constituents. US Geological Survey.

APPENDIX LEGEND

Appendix 1. Summary of all geochemical and isotope data collected for this project.